

ABSTRACT

Title of Thesis: ENZYME INHIBITION IN MICROFLUIDICS
FOR RE-ENGINEERING BACTERIAL
SYNTHESIS PATHWAYS

Dean Larios Berlin,
Masters of Science, 2009

Directed By: Professor Gary W. Rubloff
Department of Materials Science and Engineering
and the Institute for Systems Research

Enzyme-functionalized biological microfluidic (EF-BioMEMS) systems are an emerging class of lab-on-chip devices that manipulate enzymatic pathways by localizing reaction sites in a microfluidic network. An EF-BioMEM system was fabricated to demonstrate biochemical enzyme inhibition. Further, design optimizations to the EF-BioMEM system have been proposed which improve system sensitivity and performance.

The *pfs* enzyme is part of the quorum-sensing pathway that ultimately produces the bacterial signaling molecule AI-2. An EF-BioMEM system was fabricated to investigate the *pfs* conversion activity in the presence of a transition state analogue inhibitor. A reduction in enzyme conversion was measured in microfluidics for increasing inhibitor concentration that was comparable to the response expected on a larger scale. This EF-BioMEMS testbed is capable of investigating other compounds that inhibit quorum sensing.

Design improvements were demonstrated that improve overall system responsiveness by minimizing unintended reactions from non-specifically bound enzyme. EF-BioMEMS signal-to-background performance increased from 0.72 to 2.43.

ENZYME INHIBITION IN MICROFLUIDICS FOR RE-ENGINEERING
BACTERIAL SYNTHESIS PATHWAYS

By

Dean Larios Berlin

Thesis submitted to the Faculty of the Graduate School of the
University of Maryland, College Park, in partial fulfillment
of the requirements for the degree of
Masters of Science
2009

Advisory Committee:
Professor Gary W. Rubloff, Chair
Professor William E. Bentley
Professor Joonil Seog
Professor Reza Ghodssi

© Copyright by
Dean Larios Berlin
2009

Acknowledgements

I would like to thank my family who has supported me through this process, and especially my wife, Jenny Larios Berlin.

All of the members of the Rubloff group have provided valuable suggestions and advice, but I want to especially thank Dr. Susan Buckhout-White and Dr. Xiaolong Luo. Some of this work was done in collaboration with Dr. Luo.

My Thesis Advisory Committee deserves recognition for their review of my material, and the insightful comments and suggestions offered during my Thesis Defense. Additionally, I would like to extend my gratitude to Dr. Gregory Payne for his comments on enzyme inhibition analysis.

I would like to thank Dr. Vern Schramm at the Albert Einstein College of Medicine at Yeshiva University in New York for kindly providing a quantity of the MT-DadMe-Immucillin-A inhibitor in sufficiently high concentration to allow for all the experiments in this research.

This work was performed on the campus of University of Maryland, College Park. The microfabrication was done in the FabLab facility of the Maryland Nanocenter. The enzyme preparation was done in the Bentley Lab, the enzyme conversion in microfluidics was done in the Rubloff Lab, and the HPLC analysis was done in the Payne Lab.

This work was supported in part by the Robert W. Deutsch Foundation, the NSF IMI program under DMR023129, the Nation Science Foundation Emerging Frontiers in Research and Innovation (NSF-EFRI) program under NSF-SC03524414, the USDA, and the Laboratory for Physical Sciences.

Section 1 Cost Analysis.....	51
Chapter 7: References.....	53

List of Figures

Figure 1: Parasitic reactions in microfluidics due to enzyme trapped in interconnect reservoirs and non-specifically bound on microchannel walls. (a) <i>pfs</i> enzyme converts SAH substrate into products SRH and adenine. (b) Electrical signal-guided assembly of <i>pfs</i> -chitosan conjugate onto a localized assembly electrode in a microchannel followed by buffer rinsing. (c) Sequential enzymatic reaction in continuous flow in the microchannel. (d) Parasitic reactions in reservoirs and on microchannel wall as well as programmable reactions on localized enzyme assembly site.....	4
Figure 2: Quorum-sensing pathway to produce AI-2 signaling molecule ^[50]	4
Figure 3: (a) MT-DadMe-Immucillin-A transition state analogue <i>pfs</i> inhibitor, (b) MTAN-catalyzed hydrolysis of MTA (aka SAH) and the dissociative transition state of the reaction Features of the transition state which distinguish it from the substrate are shown in blue,.....	8
Figure 4: Transparency Mask Set for (a) Electrodes, and (b) Microchannels.....	10
Figure 5: Microfluidic Chip (a) showing microchannel with incorporated gold electrodes, (b) photograph of microfluidic chip with multiple channels, electrode termini and inserted tubing, (c) shown with 50ml Falcon tube that was used for transportation and storage.....	13
Figure 6: Typical HPLC elution plot.....	18
Figure 7: Sample collection schedule.....	19
Figure 8: SAH peak area for each inhibitor concentration. Each colored bar represents a sample collection of 30 minutes duration. Key: Sample 1 (blue); Sample 2 (red); Sample 3 (yellow).....	20
Figure 9: Microfluidic enzyme conversion in the presence of inhibitor.....	21
Figure 10: Chitosan electrodeposition and <i>pfs</i> -chitosan conjugation, Lewandowski experimental setup ^[33]	22
Figure 11: Reaction Rates, “CSTR”-like conditions.....	24
Figure 12: Interaction volume (not to scale).....	25
Figure 13: Relative Reaction Rates: Microfluidic Chip vs. “CSTR”-like calculations.....	27
Figure 14: Eliminating interconnect reservoirs by aligners on prototype mold to guide microfluidic packaging. (a) Aligners on prototype mold. (b) Packaging way #1: punch holes via PDMS followed by coupler insertion. (c) Packaging way #2: punch holes via PDMS followed by tubing insertion. (d) Packaging way #3: align couplers for PDMS curing followed by coupler removal and tubing insertion.....	33
Figure 15: Device and packaging. (a) Fabricated aligners on prototype mold. (b) Blue dye solution occupying a leak-tight cross-channel device. PE tubing was inserted. In experiment, enzyme solution for post-fabricated assembly flowed A→C, and substrate solution (SAH) subsequently flowed B→D.....	35

- Figure 16: The residence time distribution for channels with, and without, reservoirs. Dye solution was monitored over electrode patches 12mm downstream the microchannels. (a) With reservoir. Dye intensity increasing from 10% to 90% takes 61 sec in experiment and 75 sec in simulation. (b) Without reservoir. Dye intensity increasing from 10% to 90% takes 32 sec in experiment and 25 sec in simulation. (c) The simulated difference of intensity change from the interconnect configuration with, and without, reservoir.38
- Figure 17: Minimization of parasitic reactions. To test the background signal by non-specifically bound enzyme, *pfs* enzyme solution was introduced without electro-assembly followed by buffer rinsing, then enzymatic substrate SAH was introduced and collected downstream to be analyzed by HPLC. (a) → (b) Eliminating dead volume in interconnect reservoir and thereby eliminating homogeneous reactions). (b) → (c) Eliminating non-specific binding of enzyme to channel walls and thereby minimizing heterogeneous reactions.40
- Figure 18: Background signals (parasitic enzymatic conversion) at different flow rates. *pfs* enzyme solution was introduced without electro-assembly followed by buffer rinsing, then enzymatic substrate SAH was introduced and collected downstream to be analyzed by HPLC. Legend: 1-ch_w/ res.: single channel with interconnect reservoirs (blue); 1-ch_No res.: single channel without interconnect reservoirs (purple); X-ch_No res: cross-channel without interconnect reservoirs (red).41
- Figure 19: Total conversions in devices with electrodeposited *pfs*. Conversion by non-specifically bound enzymes is in blue, and conversion by site-specifically assembled enzymes is in red. For the non-specific conversion, no electrical signal was applied (no *pfs*-chitosan conjugate deposited). For the total conversion, an electrical signal of 3A/m^2 current density was applied for 4min (*pfs*-chitosan conjugate assembled onto 0.75 mm^2 sites). Enzymatic reaction was performed at $0.4\mu\text{L/min}$ flow rate. .43

List of Equations

- Equation 1: Inhibitor dissociation constant6
- Equation 2: Enzyme conversion computation 19
- Equation 3: Competing Reaction Pathways23
- Equation 4: Competitive Inhibition. K_M is the equilibrium constant, $[S]$ is the SAH substrate concentration, $[I]$ is the MT-DadMe inhibitor concentration, K_I is the inhibition constant, v_0 is the initial rate in the absence of the inhibitor, and v'_0 is the initial rate in the presence of the inhibitor.24
- Equation 5: Reaction rate in microfluidic chip26
- Equation 6: Final SRH concentration, as a function of enzymatic conversion26

List of Tables

Table 1: Types of reversible enzyme inhibition	6
Table 2: Microfabrication of microfluidic chip	11
Table 3: Reaction rate data for microfluidic enzyme conversion in the presence of inhibitor	26
Table 4: Chemicals and Materials List	46
Table 5: Manufacturing Cost Analysis	52

Chapter 1: Overview: Biological Enzyme-functionalized Microfluidic Systems

Enzyme-functionalized biological microfluidic systems (EF-BioMEMS) are an emerging class of lab-on-chip devices that manipulate enzymatic pathways by localizing reaction sites in a microfluidic network. The motivation of this present work is to fabricate an EF-BioMEMS that is capable of screening enzyme inhibitor compounds, and investigating design optimizations that improve the signal-to-background performance of the system.

The requirements of an EF-BioMEMS device are incorporation of active enzyme molecules, spatial localization of the enzyme on specific reaction sites, minimal contribution from non-specifically localized enzyme, and a method to introduce the reaction precursors and recover the reaction products. Researchers at University of Maryland has previously employed chitosan as biological interconnect to spatially assemble active enzymes in microfluidic channels ^{[38][39]}. Chitosan is an amine-rich polysaccharide whose solubility is pH-responsive. Its abundant amine groups allow for enzyme conjugation using tyrosine-tag based chemistry, while its pH responsiveness allows it to be electrodeposited on a cathode inside the microchannel.

Section Chapter 2: (“An EF-BioMEM system to Investigate Enzyme Inhibition”) of this present work describes an EF-BioMEMS device that is capable of meeting these requirements, and in this present has been used to investigate the biochemical inhibition of an enzyme in the bacterial quorum-sensing pathway. It will be shown that the enzyme

conversion activity decreased in a manner comparable to that observed in larger-scale well-mixed experimental configurations.

Section Chapter 3: (“Design Optimizations for EF-BioMEMs”) of this thesis describes key design improvements to that reduce the unintended side reactions that degrade the system’s signal-to-background performance. These unintended reactions take place in the homogenous phase (liquid), where active enzyme may become trapped in dead-volume sections of the device, or in the heterogeneous phase (on a surface), where active enzyme may be bound at locations other than the electrode reaction site. Modifications in the fabrication technique and the geometry of the device are explored, and shown to reduce the impact of these unintended side reactions on the overall system performance.

Chapter 2: An EF-BioMEM system to Investigate Enzyme

Inhibition

Section 1 Introduction

Microfluidic chips and polydimethylsiloxane (PDMS) soft lithography fabrication have reduced the size, reagent quantity, and cost of many standard biochemical analytical protocols, by handling nanoliter volumes ^{[10][19]}. Biological micro-electromechanical systems (bioMEMS) are an important subset of these devices that are able to recreate biomolecular reaction pathways. Of particular interest are pathways that play a critical role in the functionality, and behavior of living cells. Enzyme catalysis is central to many of these pathways, and accordingly it has been a major goal to develop means to isolate enzymes at specific locations in a microfluidic system, and confirm that their catalytic

action is maintained in this artificial setting. This would provide an attractive testbed for understanding the details of reaction pathways and kinetics, and for identifying means to modify pathways (e.g., for discovery of a drug that can significantly suppress, enhance, or modify the dominant pathway).

Our group has demonstrated bioMEMS technology that enables the programmable assembly of biomolecules on localized assembly sites in microchannels using electrodeposition of the amine-rich polysaccharide chitosan to direct the assembly [18][24][25]. Our group has recently demonstrated that a metabolic pathway enzyme, *S*-adenosylhomocysteine nucleosidase (*pfs*), can be assembled in this way and that its catalytic action is retained in the microfluidic environment, shown by conversion of substrate *S*-adenosylhomocysteine (SAH) into products *S*-ribosylhomocysteine (SRH) and adenine, as illustrated in Figure 1(a)-(c) [39]. This reaction step is known to be one of two enzyme reaction steps by which bacteria produce autoinducer-2 (AI-2), a small cell-signaling molecule that serves as a quorum-sensing communicator, through which bacterial populations exhibit altered phenotype (Figure 2). Our ultimate goal is to use the EF-BioMEMs environment as a testbed for discovery of molecules that inhibit quorum sensing. These compounds would be good candidates for a new type of antimicrobial drug that would work by interfering with bacterial communication, rather than by killing bacteria. This strategy avoids generating drug-resistant mutations that are often the result of direct attack on the bacteria.

bacteria coordinate their behavior in response to changes in their environment. Quorum sensing is involved in regulating many of the genes associated with bacterial pathogenesis ^{[1][26][39][28][30][31]}. Inhibition or knockdown of enzymes in this pathway represents new opportunities for antimicrobial drugs that target population phenotype as opposed to essential biological functions.

This strategy employs biochemical inhibitors to reduce the conversion activity of the *pfs* enzyme to inhibit the product of AI-2 precursors. Enzymes are three-dimensional molecules that have active sites that are receptive to the particular molecular geometry of the substrate. When the substrate docks in the active site, the enzyme rapidly undergoes a reversible conformational change which catalyses the conversion of the substrate into the product. The product vacates the active site, and the enzyme reshapes ready for another substrate molecule. Enzyme inhibition can proceed in a variety of ways, which fall into two classes: reversible and irreversible inhibition. In reversible enzyme inhibition the inhibitor participates in a rapidly established, reversible equilibrium with the enzyme or enzyme-substrate complex. This process can be modeled using Michaelis-Menten equations. Irreversible inhibition occurs when the enzyme undergoes permanent modification to their active sites through covalent bonding, or the enzyme is decomposed. This type of inhibition cannot be modeled using Michaelis-Menten formalism, and is not the subject of this study ^[35].

The three types of reversible inhibition are: competitive inhibition, where the inhibitor competes with the substrate for access to the active site of the enzyme; uncompetitive inhibition, where the inhibitor binds to the enzyme-substrate complex to prevent product formation; and noncompetitive inhibition, where the inhibitor can bind to

both the free enzyme or the enzyme-substrate complex ^[35]. These types of reversible inhibition are shown in Table 1, where [E], [S], [I], [ES], [EI], [ESI] and [P] refer to the concentrations of enzyme, substrate, inhibitor, enzyme-substrate complex, enzyme-inhibitor complex, enzyme-substrate-inhibitor complex, and product, respectively. The key metric for an inhibitor is the dissociation constant of the inhibition reaction, K_I , which is analogous to the binding affinity (i.e. smaller value means a stronger bond). The dissociation constant for competitive inhibition is defined in Equation 1.

$$K_I = \frac{[E][I]}{[EI]}$$

Equation 1: Inhibitor dissociation constant

The inhibitor discussed in this present work is a substrate analogue (i.e. a “lookalike”) that participates in competitive inhibition with the SAH substrate.

Table 1: Types of reversible enzyme inhibition

Uninhibited Reaction	$E + S \rightleftharpoons ES \rightleftharpoons E + P$
Competitive Inhibition	$E + I + S \rightleftharpoons EI + S$
Uncompetitive Inhibition	$E + I + S \rightleftharpoons ES + I \rightleftharpoons ESI$
Noncompetitive Inhibition	$E + I + S \rightleftharpoons ES + I \rightleftharpoons ESI$ $E + I + S \rightleftharpoons EI + S$

Other researchers have investigated the integration of enzyme components into microfluidic devices. Holden et al. have demonstrated site-specific enzyme patterning in microfluidic channels using photoimmobilization ^[41]. Ismagilov et al. have immobilized β -galactosidase enzyme molecules in agarose gels formed within intersecting microfluidic channels ^[42], which they demonstrate to be catalytically active by introducing X-gal substrate. Mao et al. have demonstrated phosphatase enzyme

immobilization by streptavidin binding to a biotinylated membrane in their microfluidic device. They further demonstrate enzyme kinetics by varying substrate concentration to construct Lineweaver-Burke plots and extract the v_{max} and K_M [43]. Fluorescence ELISA has been demonstrated by Eteshola and Leckband in microfluidics to be able to quantify the IgM sheep antibody down to nanomolar sensitivities [44]. Since ELISA depends critically upon enzyme immobilization to affix the complementary antigen, this study represented the replication of a common lab-bench procedure in an enzymatic microfluidics system.

As stated, the strategy to prevent quorum sensing is to inhibit the enzymes involved in the synthesis of the signaling molecule, AI-2. Of the two enzymes in the pathway, *pfs* and *luxS*, the *luxS* enzyme is less stable and not able to be readily electrodeposited within the microfluidic device, so the focus has been on inhibiting the *pfs* enzyme. Despite this limitation for microfluidic assembly, a literature survey did uncover work by Alfaro et al. and Shen et al. that describe the synthesis of *luxS* substrate analogue inhibitors [50][51]. Cornell et al. catalogs twenty-eight substrate analogues as potential inhibitors (in this study *pfs* is referred to as MTAN or 5'-Methylthioadenosine nucleosidase), but not all the K_I values are reported [52]. Of the values reported the dissociation constants ranged from 20nM to 750nM.

The most extensive work in the field of synthesizing *pfs* inhibitors has been done by Schramm et al. Their research has identified listed several other picomolar and femtomolar *pfs* inhibitors [34][45][46][47][48], with exceedingly tight binding constants. In a single paper, the team synthesized 51 subtly distinct substrate analogues by substituting key ligands on the SAH compound [34]. From this wide array, the tight-binding *pfs* (aka

MTAN) inhibitor called MT-DadMe-Immucillin-A (MT-DadMe) was selected (Figure 3). The name “MT-DadMe-Immucillin-A” refers to the location of the ligand substitution. The full name is 5'-methylthio-DADMe-Immucillin-A (3R,4S)-1-[(9-deazaadenin-9-yl)methyl]-3-hydroxy-4-(methylthiomethyl)pyrrolidine. MT-DadMe was chosen primarily because it was a tight-binding inhibitor (equilibrium dissociation constant $K_i^* = 2\text{pM}$)¹ and so would have a strong chance of producing measurable inhibition. It was also the only compound that Dr. Schramm had available for shipping. MT-DadMe is a formally transition state analogue, which means it closely mimics the structure of the transition-state of the natural substrate, SAH, and can therefore achieve a very tight enzyme binding.

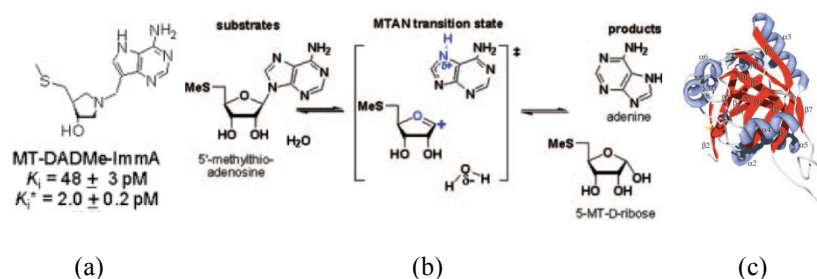


Figure 3: (a) MT-DadMe-Immucillin-A transition state analogue *pfs* inhibitor, (b) MTAN-catalyzed hydrolysis of MTA (aka SAH) and the dissociative transition state of the reaction. Features of the transition state which distinguish it from the substrate are shown in blue, (c) SAH – MT-DadMe-Immucillin-A complex [48]

¹ In the case of slow-onset tight binding inhibition, such as this, the inhibitor-enzyme binding occurs in two phases. In the first phase, the inhibitor binds reversibly to form the EI complex (K_i). In the second phase, the EI complex undergoes a conformational tightening to bind the inhibitor even further (K_i^*). For MT-DadMe, the functional dissociation constant is given by K_i^* .

Section 3 Microfluidic Chip Design and Fabrication

Sub-section 1 Design Objectives

The chip was designed with nine (9) independent flow channels, and six electrodes per channel. This allows five separate electrodeposition events to take place simultaneously within the same flow channel, while the sixth electrode is used repeatedly as the counter electrode. The layout design of the electrode termini was inspired from DRAM chips, so that in the future it might be used as cartridges in a handheld control device. The envisioned application is as a disposable testing cartridge capable of performing a variety of operations that involve enzyme reactions for in the roles of drug compound screening, small-scale manufacturing of short-lived signal products, or analyzing the interaction of an analyte with a fixed metabolic pathway. The cartridges could be premade, and in a sealed ready state for enzyme functionalization and use.

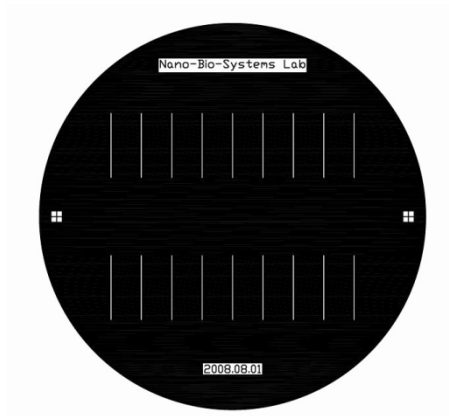
The mask set used is shown in Figure 4:



(a)

Electrode Mask

This bright-field mask allows for the patterning of two sets of 54 addressable, 1mm^2 electrode pads. Au/Cr electrodes are etched through Shipley 1813 positive photoresist hardened by UV exposure



(b)

Microchannel Mask

This dark-field mask allows for the patterning of two sets of nine $0.5 \times 18\text{mm}$ positive relief molds from UV-exposed SU8-50 negative photoresist. Microfluidic channels were cast in PDMS casts from these SU8-50 relief molds.

Figure 4: Transparency Mask Set for (a) Electrodes, and (b) Microchannels

Sub-section 2 Fabrication Procedure

The microfluidic chip was built using soft lithographic techniques. The microfluidic channels are designed to allow for the electrodeposition of enzyme-chitosan conjugate at specific locations, and then to allow for enzyme inhibition by flowing of inhibitor compounds. The procedure is detailed in Table 2 below:

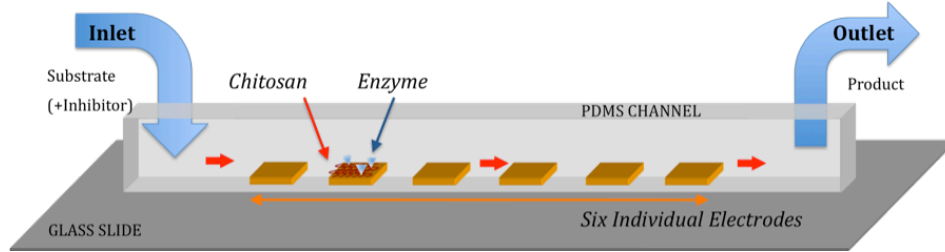
Table 2: Microfabrication of microfluidic chip

Step	Operation	Approx. Time
1	Transparency mask fabrication	
1-1	Dark field microchannel mask design using AutoCAD	2 days
1-2	Bright field electrode mask design using AutoCAD	
	Masks are printed on Mylar (transparency masks) by an external vendor (e.g. CAD/Art Services)	3 days
2	SU8 positive relief wafer formation	
2-1	Remove SU-8 50 from refrigerator at least 2 hours before process	
2-2	Clean the wafer with Acetone, Methanol, IPA cleaning and DI water rinsing, if not cleaned by piranha solution	2 min
2-3	Dehydrate the wafer on a hot plate (200°C, 30 min, auto-off)	30 min
2-4	Prepare hotplates 65°C & 95°C	5 min
2-5	Cover 2/3 of wafer surface (~4 ml) with SU-8 while wafer is on spinner	1 min
2-6	Spin a 50 µm thick SU-8 50 film (100 rpm/sec ramp to 500 rpm, 10 sec; 300 rpm/sec ramp to 2000 rpm, 30 sec)	1 min
2-7	Pre-bake SU-8 50 on 65°C hotplate, 6min then 95°C for 20 min	26 min
2-8	Expose with 400 mJ/cm ² UV dose through Microchannel mask	15 min
2-9	Post Exposure Bake SU-8 50 on 65°C hotplate for 1min ramp at 200°C/hr to 95°C, hold at 95°C hotplate for 5 min, auto off	30 min
2-10	7min in SU-8 Developer, rinse briefly with IPA and gently dry with N ₂	10 min
2-11	Hard bake the wafer at 150°C for 5 min, 300°C/hr, auto-off	30 min
2-12	This produces the SU-8 positive relief wafer	
3	PDMS Processing	
3-1	Prepare 65°C oven	
3-2	Mix 10:1 ratio (prepolymer: curing agent) PDMS	10 min
3-3	Pour PDMS over SU-8 positive relief wafer, degas under vacuum	25 min
3-4	Cure in oven until solid	2 hrs
3-5	This produces the PDMS mold, but still attached to the SU-8 positive relief wafer	

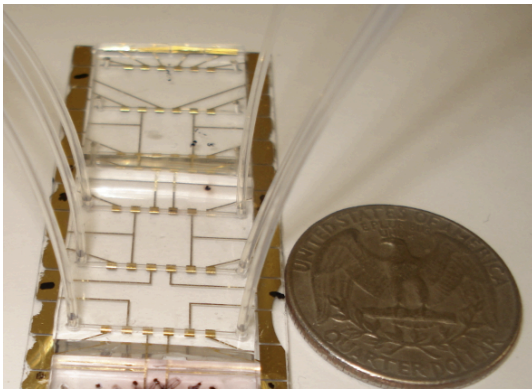
4	Gold electrode fabrication	
4-1	Clean glass substrate slides in piranha solution right before evaporation	
4-2	Load glass substrate slides into thermal evaporator	10 min
4-3	Thermally evaporate $\sim 200\text{\AA}$ of Chromium, as an adhesion layer between the gold and the glass	15 min
4-4	Thermally evaporate $\sim 2000\text{\AA}$ of Gold, as the conductive layer	15 min
4-5	Cover in Shipley 1813 photoresist, spun at 5000rpm, 30sec	1 min
4-6	Soft bake (100°C , 1 min)	2 min
4-7	Expose with 200 mJ/cm^2 UV dose through Electrode mask	10 min
4-8	Develop photoresist in Shipley 352 developer, and rinse	2-5 min
4-9	Hard bake at 120°C for a few minutes	3 min
4-10	Etch Gold layer in Transene TFA etchant, $\sim 100\text{sec}$	2 min
4-11	Etch Chromium layer in Transene 1020 etchant, $\sim 5\text{-}10\text{sec}$	1 min
4-12	Clean wafer with photoresist stripper (60°C , 5 min), then rinse in water	10 min
4-13	This produces the gold electrodes on the glass substrates	
5	Final assembly	
5-1	Using razor blade and spatula, carefully peel off PDMS mold from SU-8 positive relief wafer	
5-2	Holes are reverse-punched for the fluid tubing interface, using 0.75mm puncher	5 min
5-3	The PDMS layer and the gold-coated glass substrates are placed in the O_2 plasma asher	
5-4	Exposure to plasma: 450mTorr, 20W, 20sccm O_2 , 30 sec	5 min
5-5	Immediately after removal from plasma, the two surfaces are placed in contact and a permanent bond is rapidly formed. The bond sets overnight	24 hrs
5-6	Insert tubing into punched holes of the fluid channel (use 0.558mm ID/ 1.0668mm OD PTFE tubing), and connect to the syringe pump	10 min

Sub-section 3 Final Microfluidic Chip

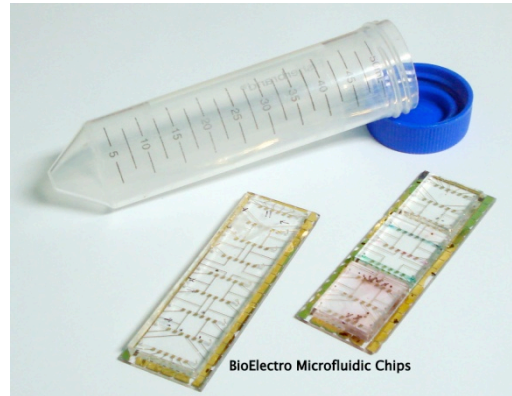
The final microfluidic chip is shown below in Figure 5.



(a)



(b)



(c)

Figure 5: Microfluidic Chip

(a) showing microchannel with incorporated gold electrodes, (b) photograph of microfluidic chip with multiple channels, electrode termini and inserted tubing, (c) shown with 50ml Falcon tube that was used for transportation and storage

The final chip, as shown in Figure 5 (b) and (c), is compact, with nine (9) independent microfluidic channels with fifty-four (54) addressable electrode locations, supplied with fluid by nine (9) pairs of inlet-outlet tubing ports all on a single 1”x3” typical wafer slide. The final chip was robust and could be easily stored on the shelf, or transported safely in common 50mL Falcon tube. The terminus of each addressable electrode in the chip was designed to be easily accessed using Alligator clips and a

standard power control unit. The batch fabrication techniques employed allowed many chips to be made in about 2 days of single-person labor using pre-designed mask sets. The materials choice and scale of manufacture with estimated cost of less than \$10 per chip.

Section 4 Experimental Methods

The impact of the MT-DadMe inhibitor on *pfs* enzyme activity in the EF-BioMEM system was tested using the experimental design described below:

1. Preparation

- a. The microfluidic chip was assembled with tubing and connected to a syringe pump.
- b. The channel was flushed with HCl at 10 μ L/min for at least 10min to remove any contaminants and denature any enzyme from a previous run.
- c. The channel was flushed with Milk blocking solution at 10 μ L/min for at least 2hrs to discourage non-specific chitosan bonding, and stabilize pH near the optimum value for enzyme catalysis.
- d. The channel was flushed with deionized (DI) water at 10 μ L/min for at least 30min to remove the Milk blocking solution.
- e. The *pfs*-chitosan tyrosine conjugate was brought to room temperature.

2. Electrodeposition

- a. The microchannel was filled with *pfs*-chitosan tyrosine conjugate solution at 5 μ L/min for enough time to fill the microchannel.

- b. An air bubble was introduced between the slug of conjugate solution, and the succeeding slug of PBS. The air bubble was advanced to be just ahead of the depositing electrode so that the chitosan electrodeposition reaction can be rapidly terminated.
- c. The flow was stopped.
- d. Electrodeposition occurred by current control set to be 3A/m^2 ($1.5\mu\text{A}$ for an electrode area of 0.5mm^2) by a Keithley 2600 SourceMeter for 4min. The depositing electrode was set as the cathode, and the counter electrode was set as the anode.
- e. Flow was restarted so that PBS flowed through the microchannel at $5\mu\text{L}/\text{min}$ about 5 min.
- f. The tubing was changed to avoid cross-contamination.

3. Enzyme Conversion

- a. The microchannel was flushed with 1mM SAH substrate at $4\mu\text{L}/\text{min}$ for 1hr to prime the conversion. The resulting product from this period was discarded.
- b. Batches of product were collected from SAH substrate flow ($4\mu\text{L}/\text{min}$) every 30min, for 1.5hr to yield three vials of $120\mu\text{L}$ each.
- c. Each sample vial was stored in a vat of ice to quench any lingering enzymatic conversions and prevent product denaturation.
- d. A sample of unconverted 1mM SAH solution was also collected as a standard.
- e. The tubing was changed to avoid cross-contamination.

4. Enzyme Inhibition

- a. 1mM SAH substrate and inhibitor solution were thoroughly mixed together to achieve the desired concentration. The mixture was brought to room temperature.
- b. The following MT-DadMe inhibitor concentrations were tested:
 - i. 2500nM
 - ii. 1000nM
 - iii. 500nM
 - iv. 375nM
 - v. 250nM
 - vi. 125nM
- c. The microchannel was flushed with SAH-inhibitor solution at 4 μ L/min for 1hr to prime the conversion. The resulting product from this period was discarded.
- d. Batches of product were collected from SAH-inhibitor flow (4 μ L/min) every 30min, for 1.5hr to yield three vials of 120 μ L each.
- e. Each sample vial was stored in a vat of ice to quench any lingering enzymatic conversions and prevent product denaturation.
- f. The tubing was changed between experiments to avoid cross-contamination.
- g. All product vials were collected together and frozen until ready for HPLC measurement.

5. Metrology

- a. Samples were measured in HPLC.
- b. The SAH peak area was used as the metric to measure enzyme conversion.

A few notes about the procedure:

First, care was taken to always replace the tubing, as this is a major contributor to contamination. Enzyme-chitosan conjugate or inhibitor can bind non-specifically to the interior walls of the tubing and interact with inhibitor to cause uncontrolled side reactions.

Second, electrodes were only used once as deposition electrodes. This was done so that each electrode was fresh for chitosan deposition and successive depositions were not complicated by previous actions. This means that each channel was, at most, five times since there were six electrodes per channel, and one electrode was designated as the control terminal. The microchannel was cleaned with HCl and buffer between each deposition and conversion process.

Third, SAH was flowed for 1hr to prime the enzyme conversion because it had been observed that conversion products collected from the first 30-45minutes were erratic, with conversion rates varying by large amounts. It appeared that after 1hr, the conversion rate stabilized and became more repeatable. The schedule in Figure 7 was followed for sample collection.

Section 5 Results

High Performance Liquid Chromatography (HPLC) was used to determine the relative components of the product sample. Different compounds have different elution

times based upon their affinity with the stationary phase of chromatography column. In this case, the elution time for adenine is 4.8min, the elution time for SRH is 4.3 min, and the elution time for SAH is 8.4min [32]. By comparing the SAH peak area in a converted sample to that of the unconverted, it is possible to determine the amount of SAH remaining in the sample, and therefore the degree of enzymatic conversion. The SRH peak was not used because it is of relatively low intensity compared to the SAH peak, and its elution time is too close to that of adenine to avoid being confused. A typical HPLC elution plot is shown in Figure 6 below. The y-axis measures the counts received by the absorbance detector, and it is common for this reading to have a baseline offset from zero (as shown in Figure 6), as this depends on the most recent zeroing of the detector. This is easily accounted for by shifting the data to the correct zero line.

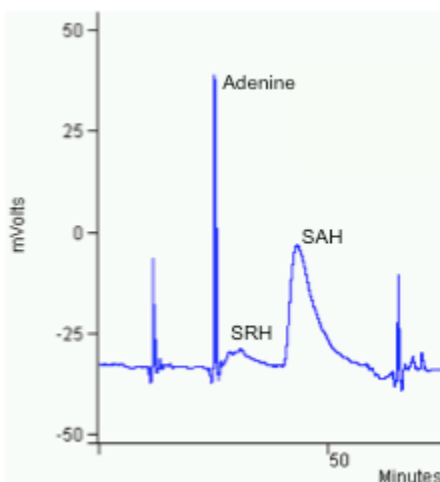


Figure 6: Typical HPLC elution plot

For each inhibitor concentration, the SAH peak area was plotted for the case with inhibitor mixed with substrate (Inh.), for the case of substrate alone (UnInh.), and for the associated inlet SAH concentration (Std.) in Figure 8. The sample collection proceeded according to the following schedule in Figure 7. This schedule includes a 1hr

	Sample 1 (30min)	Sample 2 (60min)	Sample 3 (90min)
UnInh.	392,055	2,192,623	1,624,023
Inh.	2,966,045	2,864,477	2,918,340
Std.	2,989,061		

a)

	Sample 1 (30min)	Sample 2 (60min)	Sample 3 (90min)
UnInh.	158,563	8,070,588	8,767,815
Inh.	12,880,576	17,489,407	19,685,766
Std.	20,820,722		

b)

	Sample 1 (30min)	Sample 2 (60min)	Sample 3 (90min)
UnInh.	133,093	792,613	355,135
Inh.	8,141,117	2,398,274	2,696,882
Std.	14,476,588		

c)

	Sample 1 (30min)	Sample 2 (60min)	Sample 3 (90min)
UnInh.	1,521,344	671,796	1,655,834
Inh.	1,054,332	987,669	952,188
Std.	12,758,000		

d)

	Sample 1 (30min)	Sample 2 (60min)	Sample 3 (90min)
UnInh.	556,074	766,851	611,934
Inh.	-400,544	-80,109	No data
Std.	8,010,882		

e)

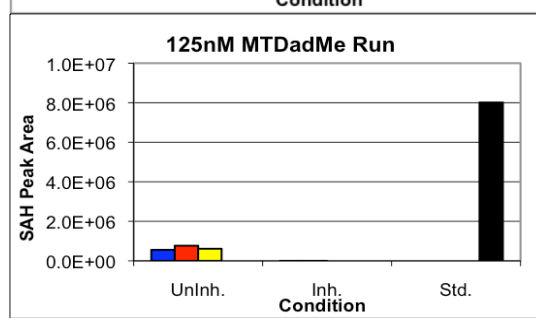
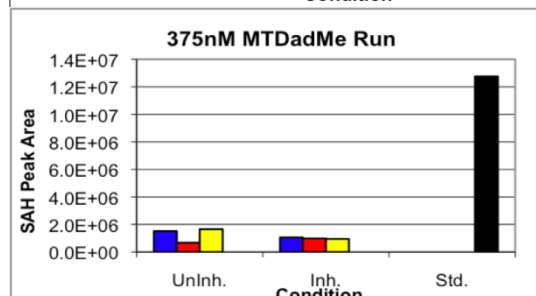
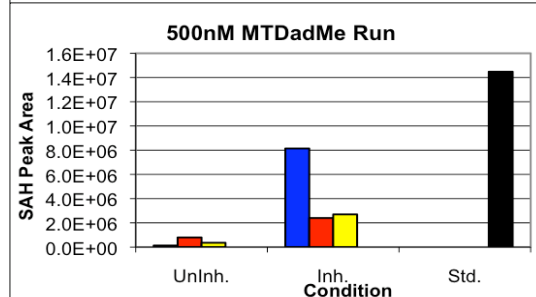
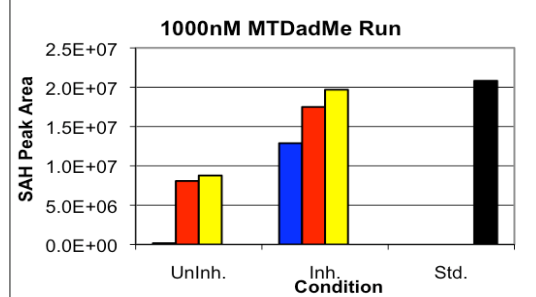
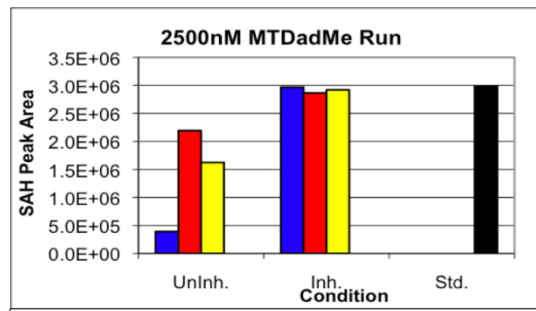


Figure 8: SAH peak area for each inhibitor concentration. Each colored bar represents a sample collection of 30 minutes duration. Key: Sample 1 (blue); Sample 2 (red); Sample 3 (yellow).

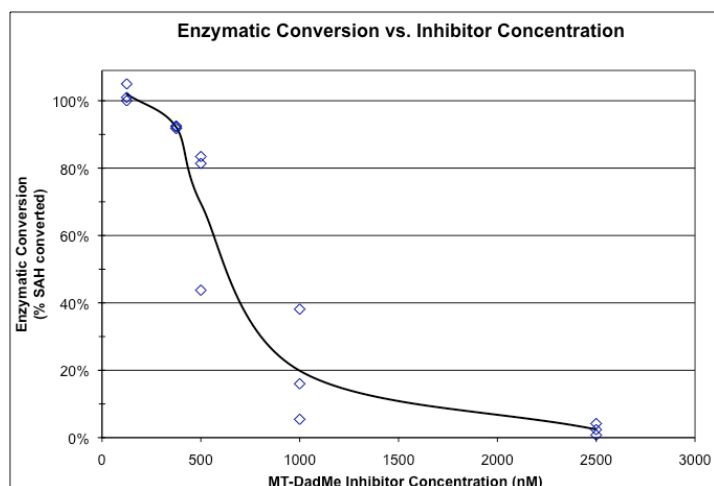


Figure 9: Microfluidic enzyme conversion in the presence of inhibitor

To address the concerns of repeatability and crosstalk between individual tests, several precautions were taken. First, the microfluidic chip design allowed each microchannel to have six individually addressable electrodes. One electrode was designated the common counter electrode (anode), with the remaining five electrodes as single-use cathodes (electrodepositing). Since the electrode was used only once for each test, it reduced the crosstalk that could occur by repeated depositions. Second, the microchannel was flushed with HCl acid after and before each test to fully dissolve and rinse any remaining chitosan, and deactivate and eliminate any residual enzyme. Third, the fluidic tubing was replaced fresh for each test to reduce the impact of non-specific binding. Additionally, these tests at different inhibitor concentrations were conducted over a span of several weeks, while the device was stored on the shelf and the biochemical fluids were stored in the refrigerator.

Section 6 Discussion

Sub-section 1 “CSTR”-like calculations

Lewandowski reports that the Michaelis-Menten, K_m , constant for *pfs* enzyme to be $K_m=0.12\pm 0.04\text{mM}$ and the maximum reaction rate for this enzyme conversion to be $v_{max}=0.11\pm 0.02\text{mM/hr}$ [33]. These values were determined using a different experimental design, as shown in Figure 10. However, the *pfs*-chitosan conjugate used by Lewandowski was prepared in the same way as the current experiment, by the same personnel.

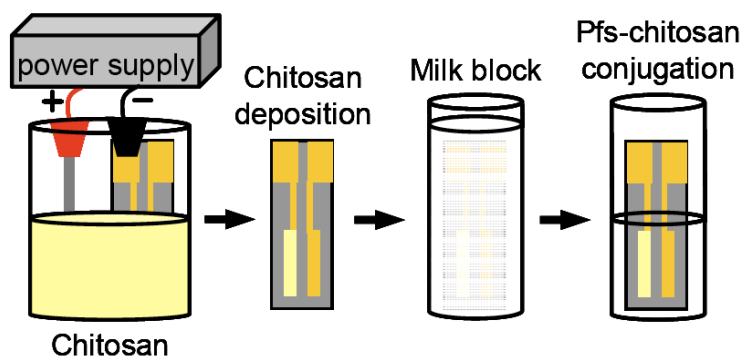


Figure 10: Chitosan electrodeposition and *pfs*-chitosan conjugation, Lewandowski experimental setup [33]

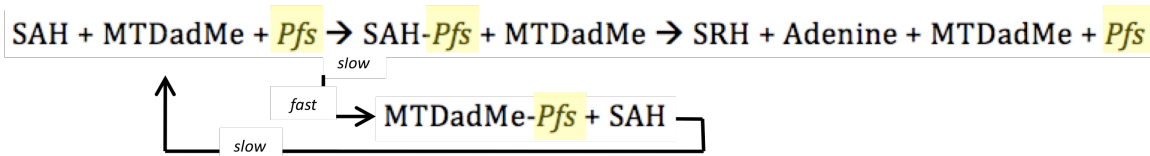
For this particular inhibitor, MT-DadMe-Immucillin-A & enzyme, Schramm et al. reports that the inhibition constant be $K_I=2\times 10^{-9}\text{mM}$, and the Michaelis-Menten constant to be $K_M=4.3\times 10^{-3}\text{mM}$ [34]. This value was determined by ultraviolet absorption using the extinction coefficients of the reaction products in volumes of 1mL at 25°C. Using *pfs*-chitosan conjugate deposited on large-scale chips, Lewandowski reports that the Michaelis-Menten, K_M , constant for *pfs* enzyme to be $K_M=1.2\times 10^{-1}\text{mM}$, and the maximum reaction rate for this enzyme conversion to be $v_{max}=0.11\pm 0.02\text{mM/hr}$ [33]. Both of these values for K_M are relatively close to each other, suggesting that while chitosan

immobilization does affect the equilibrium conditions, it is not such a strong effect to negate entirely the ability of the *pfs* enzyme to perform substrate conversion.

Since both of these referenced experimental arrangements more closely approximate a well-mixed, continuously-stirred reactor design than the microfluidic channel arrangement of the current study, the values given here represent an upper bound on the kinetics of reaction kinetics for this system. Ideally, a continuously stirred reaction design allows for all the species in the solution (i.e. enzyme, inhibitor and enzyme) to interact freely.

The type of enzyme inhibition that is occurring is competitive inhibition of the substrate (SAH) for the active enzyme (*pfs*) sites by a tight-binding substrate transition-state analog (MT-DadMe). This inhibitor binds to the enzyme, preventing it from effecting substrate catalysis. Since the binding of the analog is so strong, many substrate molecules flow by in the fluid stream unconverted.

This competitive inhibition may be described by two competing reaction pathways:



Equation 3: Competing Reaction Pathways

Using the formula, shown in Equation 4, for competitive inhibition it is possible to establish the graph of relative reaction rate shown in Figure 11.

$$\frac{v_0'}{v_0} = \frac{K_M + [S]}{K_M + [S] + K_M \frac{[I]}{K_I}}$$

Equation 4: Competitive Inhibition. K_M is the equilibrium constant, $[S]$ is the SAH substrate concentration, $[I]$ is the MT-DadMe inhibitor concentration, K_I is the inhibition constant, v_0 is the initial rate in the absence of the inhibitor, and v_0' is the initial rate in the presence of the inhibitor.

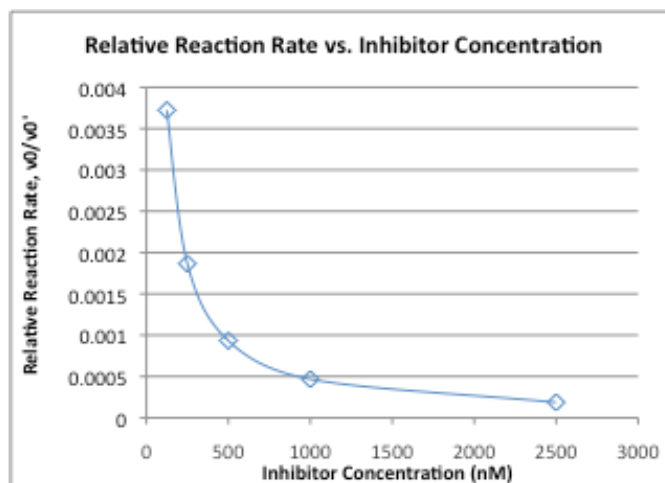


Figure 11: Reaction Rates, “CSTR”-like conditions

Sub-section 2 Microfluidic conditions

The microfluidic environment differs from the “CSTR”-like environment in crucial aspects related to the flow conditions. The microfluidic condition is under laminar constant flow conditions. This is unlike a “CSTR”-like condition, where there is a well-mixed fixed volume with no net exchange. Laminar flow conditions are marked by parallel fluid streamlines, with little chaotic mixing. This means that fresh substrate arrives continuously, and product is removed. The laminar flow conditions that present in the microfluidic channel (Reynolds number $\ll 1$) imply that only the substrate and inhibitor molecules in the flow streams near the electrode/chitosan boundary layer will interact, while the vast majority pass above the enzyme and do not interact at all. This is shown (not to scale) in Figure 12 below.

This interaction volume can be estimated based on the thickness of the deposited chitosan hydrogel matrix. Based on previous observations of dry chitosan measurements and the aqueous swell ratio, the electrodeposited chitosan is approximately 10-20 μm thick. The microchannel was fabricated to be 500 μm wide and 150 μm tall. The gold electrode area is 0.5 mm^2 ; chitosan is assumed to fully cover the electrodeposition area. The enzyme is conjugated to the chitosan hydrogel in a random fashion, with exposed enzyme on the chitosan surface and accessible enzyme within the loose hydrogel bulk. The laminar flow restricts full mixing, so only flow streams that impinge directly on the chitosan thickness, or those within the boundary layer and near to it would interact with the conjugated enzyme. Considering the low hydrogel density, and low Reynolds number flow conditions, the interaction height would be 20-40 μm . Therefore, it is estimated that only 13-26% of the total fluid volume above the electrode interacts with the conjugated enzyme.

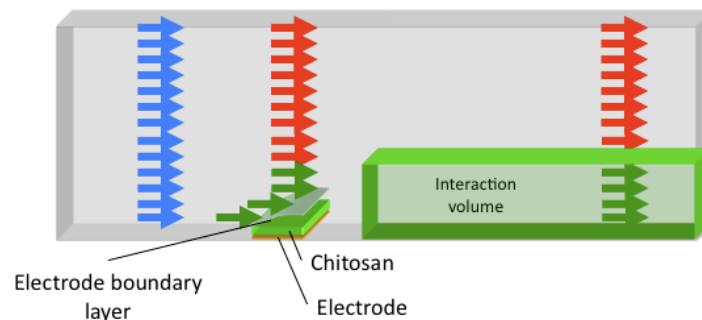


Figure 12: Interaction volume (not to scale)

This analysis from inhibitor studies done in the “CSTR”-like conditions system can be compared with the data collected in the microfluidic chip (Figure 5). It is possible to calculate the reaction rate in the microfluidic chip

$$v_{\text{microfluidic}} = \frac{[SRH]_{\text{final}} \cdot \text{FlowRate}}{\text{SampleVolume}}$$

Equation 5: Reaction rate in microfluidic chip

Recalling the *pfs* reaction equation from Figure 1, the final [SRH] concentration can be written as

$$[SRH]_{\text{final}} = \%_{\text{conversion}} \cdot [SAH]_{\text{initial}}$$

Equation 6: Final SRH concentration, as a function of enzymatic conversion

The flow through the system was fixed by syringe pump at 4μL/min, for 30min, to yield a sample volume of 120μL. The average enzymatic conversion of SAH was taken from Figure 9, which can easily be shown to be equivalent to the relative reaction rate. Collecting this data together, the reaction rate can be tabulated as shown below:

Table 3: Reaction rate data for microfluidic enzyme conversion in the presence of inhibitor

Inhibitor Concentration	Initial [SAH]	Average enzymatic conversion of SAH == Relative Reaction Rate	Final [SRH]	Reaction Rate in Microfluidic Device
125nM	1mM	103%	1.03mM	572.2nM/hr
375nM		92.18%	0.922mM	512.1nM/hr
500nM		69.52%	0.695mM	386.2nM/hr
1000nM		19.86%	0.199mM	110.3nM/hr
2500nM		2.43%	0.024mM	13.5nM/hr

Sub-section 3 Comparison of “CSTR”-like calculations and Microfluidic Conditions

It is now possible to compare the results from of *pfs* inhibition in a microfluidic environment with that of *pfs* inhibition in the “CSTR”-like conditions. This is done in Figure 13.

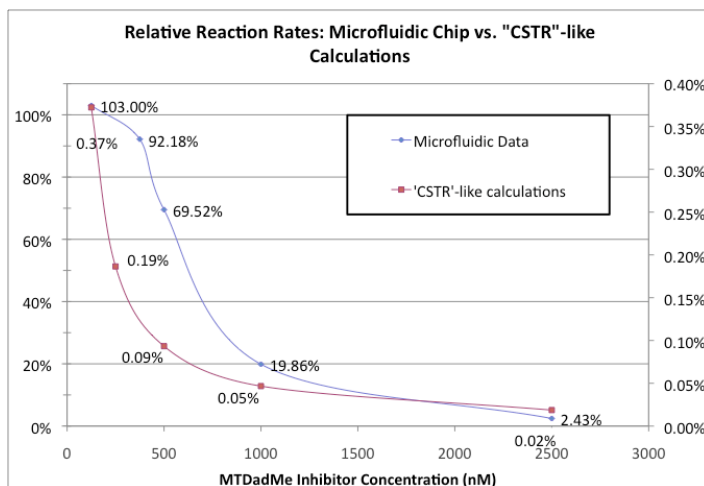


Figure 13: Relative Reaction Rates: Microfluidic Chip vs. “CSTR”-like calculations

Section 7 Conclusion

This demonstrates the design of a microfluidic chip for use in enzyme inhibitor analysis. Chitosan-conjugated *pfs* enzyme was electrodeposited within the chip in a spatially localized process that maintained enzyme conversion activity. The tight-binding substrate analogue inhibitor was used to demonstrate biochemical inhibition of *pfs* enzyme conversion activity. Analysis of the inhibition response of the experimental microfluidic data shows a decaying reaction rate with increasing inhibitor concentration. This agrees well with calculations based on “CSTR”-like conditions, and demonstrates a classic case of biochemical inhibition, where higher concentrations of inhibitor retard the reaction. This microfluidic chip can be used to screen other compounds for their efficacy as an inhibitor to the quorum-sensing pathway.

Chapter 3: Design Optimizations for EF-BioMEMs²

Section 1 Introduction

Enzyme-functionalized biological microfluidic systems (EF-BioMEMs) provide an attractive approach to understanding and modifying enzymatic pathways by separating and interrogating individual reaction steps at localized sites in a microfluidic network. Our group has previously shown that electrodeposited chitosan enables immobilization of an enzyme at a specific site while maintaining its catalytic activity ^{[33][39]}. While promising as a methodology to replicate metabolic pathways and search for inhibitors as drug candidates, these investigations also revealed unintended (or parasitic) effects, including products generated by the enzyme either (1) in the homogeneous phase (in the liquid), or (2) nonspecifically bound to microchannel surfaces. Here, EF-BioMEMs designs are reported that significantly suppress these parasitic effects. To reduce homogeneous reactions new packaging and assembly strategy have been developed that eliminates fluid reservoirs that are commonly used for fluidic interconnects with external tubing. To suppress reactions by nonspecifically bound enzyme on microchannel walls a cross-flow microfluidic network design has been implemented so that enzyme flow for assembly and substrate/product for reaction share only the region where the enzyme is immobilized at the intended reaction site.

Sub-section 1 Motivation: Reducing Unintended Enzyme Reactions

The previous section demonstrated conversion activity from chitosan-conjugated enzyme assembled in a microfluidic device. This is corroborated by other published

² Also published in Biomedical Microdevices ^[40]

studies from our group ^[39]. While these results showed clear enzyme activity at the assembled active sites, it was accompanied by notable (~15-30%) background (or “parasitic”) reaction that occurred elsewhere in the microfluidic system (signal/background ratio, or S/B, =3-6X). This is not surprising, given that the surface area and volume at the reaction site comprised only ~0.2% of the total wall area and volume of the microfluidic system. The result indicates that the active site is >1000X more efficient than unintended (parasitic) sites in the microfluidic network. These background signals appear in control experiments and are not associated with the intended catalytic action at the enzyme assembly sites. Accordingly, background reaction channels are referred to as “parasitic” in that they produce reactions that add to and interfere with efforts to localize reactions at the electrode sites.

The purpose of the present work is to reduce two significant parasitic reaction mechanisms in our EF-BioMEMs. One is a homogeneous reaction mechanism, in that substrate and enzyme react while in the fluid phase. It occurs because active enzyme is retained in reservoir areas where fluidic interconnects are made at the packaging level. The other is a heterogeneous reaction mechanism, in which enzyme nonspecifically bound to microfluidic channel walls reacts with substrate impinging from the fluid phase. These mechanisms are depicted schematically in Figure 1(d).

Sub-section 2 Eliminating reservoir dead volume

Connections between an EF-BioMEMs chip and external sources of fluids are essential to operate the chip. However, alignment of fluidic inputs/outputs (I/O's) to the microchannels can be challenging. A conventional approach is to design a larger fluidic reservoir as an interface between on-chip microfluidic channels and external fluidic

connections at the packaging level, reducing the precision needed for alignment. This approach has been used for tubing connection in microfluidics from individual microsystems ^{[2][9][11][15]} to large-scale integration ^{[17][22][23]}. The reservoirs are not readily flushed since their geometry leaves dead volume regions which entrap reactive biomolecules (e.g. enzymes) for extended periods of time, causing homogeneous parasitic reactions and altering the apparent conversion efficiency and time dependence of intended enzyme reaction steps ^{[12][16]}.

To avoid the homogenous parasitic reactions in interconnect dead volume, a new packaging technique has been implemented that involves fabricating aligners on soft lithography molds to improve the alignment capability for interfacing between in-plane microfluidic channels and external tubing. The macro-scale packaging and assembly technology issues and their effect on microfluidic performance have been reviewed in literature ^[7]. Our design eliminates the interconnect reservoirs by fabricating on-chip SU-8 aligner plugs, analogous to Si plugs made by DRIE ^[8], to guide microfluidic packaging connections. The relevant properties of PDMS that enable this technique are given elsewhere ^[17]. Here, PDMS sealing around tubing 20% larger than the nominal diameter of the hole is shown that builds on the demonstration in the literature ^[3]. Two rigid Plexiglas plates are employed to clamp the PDMS-glass chip, and stabilize the pogo pins on their electrode contacts, similar to the demonstration by Bhagat et al. where rigid clamps were employed to mechanically stabilize the tubing ^[1]. Background biochemical activity is reduced by 33% in the new design.

Sub-section 3 Reducing impact of nonspecifically bound enzyme

The presence of microfluidic channel walls with area far in excess of that of the intended enzyme reaction site is intrinsic to the geometry of EF-BioMEMs. As indicated in Figure 1(d), however, our EF-BioMEMs design employed a single channel to (1) first activate the enzyme to react with chitosan, and then deliver the enzyme-chitosan conjugate to be immobilized on the assembly site by electrical signal, and (2) subsequently to transport substrate to the active site and product away from it to a downstream collection point. This configuration exposed substrate to nonspecifically bound enzyme through the full length of the channel prior to its collection.

To reduce the contribution of enzyme nonspecifically bound on channel walls, a cross-flow EF-BioMEMs channel design is implemented. The channel that carries the enzyme-chitosan conjugate for immobilization is orthogonal to a second channel that carries substrate and product downstream to an exhaust location for analysis of enzyme conversion rate. Thus, substrate is exposed to enzyme only at the active site, suppressing the contribution of nonspecifically bound enzyme to measured conversion rates.

This experimental strategy utilizing cross-flow microchannels to separate flow directions for sequential biochemical reactions has been broadly used in DNA/protein separation^[15], droplet formation^[21] and enzymatic reaction^[2], where the cross area is the focus point for sample manipulation or for reagent introduction. In this work, the metabolic enzyme *pfs* is spatially assembled at the intersection between two flow channels so that the flow direction for enzyme assembly is separated from the subsequent flow direction for enzymatic reaction. This design enhancement is an important advance toward our goal of reconstructing multiple metabolic pathway enzymes. Spatially separating individual reaction steps in microfluidics allows for an understanding of

reaction details and testing of molecules that can modify pathways and kinetics. In drug discovery, for example, a molecular species that inhibits a bacterial signaling pathway enzyme can be a candidate for an antimicrobial drug whose action is to interfere with cell signaling or quorum sensing (more on this in Section Chapter 2:). By using a cross-flow design to separate flow directions, the non-specific heterogeneous reactions on microchannel walls are significantly suppressed and reduce the background signal by an additional 50%. Together, these EF-BioMEMs design modifications result in a combined enhancement of 3.38X in the signal/background ratio (from 0.72 to 2.43).

Section 2 Optimized Microfluidic Chip Design and Fabrication

For this work, a soft lithography molding approach was employed ^[17] to the fabrication of the EF-BioMEMs, in contrast to our previous work on enzyme reactions in BioMEMs, which incorporated SU8 sidewalls ^[16]. This accelerates development and testing of the concept, while removes some of the benefits of our earlier design ^[18].

Sub-section 1 Packaging aligners to eliminate interconnect reservoirs

To avoid homogeneous parasitic reaction in interconnect dead volume, minimal or no interconnect reservoir is desired. To achieve this goal, packaging aligners using a soft lithography molding process were designed and fabricated. As shown in Figure 14(a), packaging aligners of 500 μm in diameter were patterned from a 200 μm -thick SU-8 layer on the top of the 150 μm -thick SU-8 mold layer used to define the 500 μm -wide microchannels. A design offset of 1.07% was applied in the photomask to accommodate the shrinkage ratio of PDMS ^[13]. Figure 15(a) shows the fabricated prototype mold with packaging aligners.

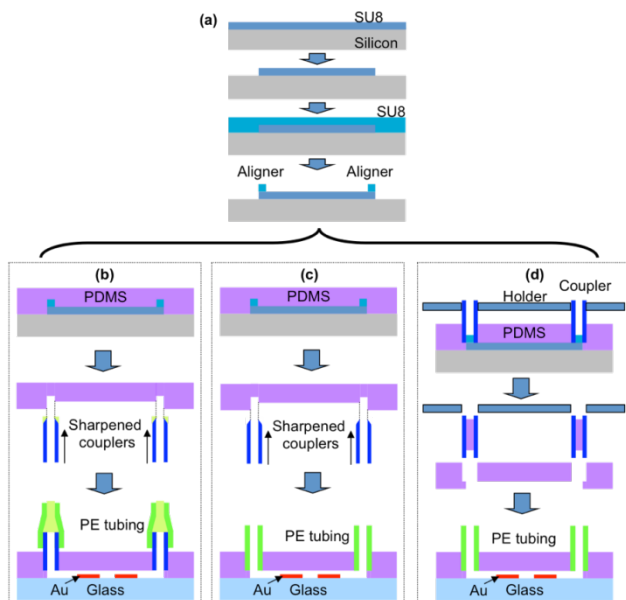


Figure 14: Eliminating interconnect reservoirs by aligners on prototype mold to guide microfluidic packaging. (a) Aligners on prototype mold. (b) Packaging way #1: punch holes via PDMS followed by coupler insertion. (c) Packaging way #2: punch holes via PDMS followed by tubing insertion. (d) Packaging way #3: align couplers for PDMS curing followed by coupler removal and tubing insertion

Three ways of PDMS curing and packaging have been explored to assemble the final chip without interconnect reservoirs to external tubing. In Figure 14(b), a sharpened coupler (fabricated in-house from a 25ga coupler, 0.020" OD) was used to punch through the 3mm-thick PDMS layer along the pits formed by the packaging aligners during the PDMS curing process. Holes for electrical contact (0.1" diameter) were also punched in the PDMS before the microchannel side was wetted with methanol and bonded to a glass slide (1"x3"). The whole chip was then sandwiched with screws between two Plexiglas clamp plates, and with pogo pins inserted through holes in the top plate for electrical connection. Finally, flat-end couplers of the same size were inserted into the punched holes and connected to external PE tubing (0.015" ID).

Figure 14 (c) shows the same strategy as Figure 14 (b) except that the external tubing was directly inserted into the punched holes in PDMS. In Figure 14 (d), couplers with inner-diameter of 0.024" (20ga, 0.036" OD) were gently placed onto the aligners of

0.5mm OD and stabilized with a Plexiglas coupling holder while the PDMS cured. Then the couplers were removed and external Microbore PTFE tubing (0.022" ID, 0.042" OD) was inserted into the well-defined connection holes (0.036" OD). Due to capillary action, couplers were normally filled with PDMS after curing, which was advantageous because it allowed a slug of PDMS to be removed, facilitating better sealing. A packaged chip following the procedure of Figure 14 (d) is shown in Figure 15(b) with blue dye flowing through the cross channel.

Finally, leak testing showed that all three strategies provide leak-tight sealing. The designs in Figure 14 (b) and (c) were predominantly used in our experiments since they minimized the dead volume between the coupler and tubing as well.

Sub-section 2 Cross-channel design to separate sequential flow directions

Cross channels (500 μ m-wide, 150 μ m-high) as shown in Figure 15 (b) were designed to separate the sequential flow direction of enzyme assembly (A \rightarrow C) from the flow direction of the subsequent enzymatic reaction (B \rightarrow D). No on-chip valves were included for this test-of-concept design. Parafilm was used to seal the connecting couplers/tubing that were not being used for a given experiment step to minimize the flow into these channels. After enzyme assembly, PBS buffer was pumped into the top three ports of the chip in Figure 15 (b) to rinse the channels. In the following experiment, substrate was continuously pumped through the reaction site at the intersection for \sim 10 hours. The serpentine channel connecting the bottom port was included to increase channel length in an efficient manner to prevent any enzyme from defusing back to the reaction site. The packaging aligners described above were also included for this cross-channel design.

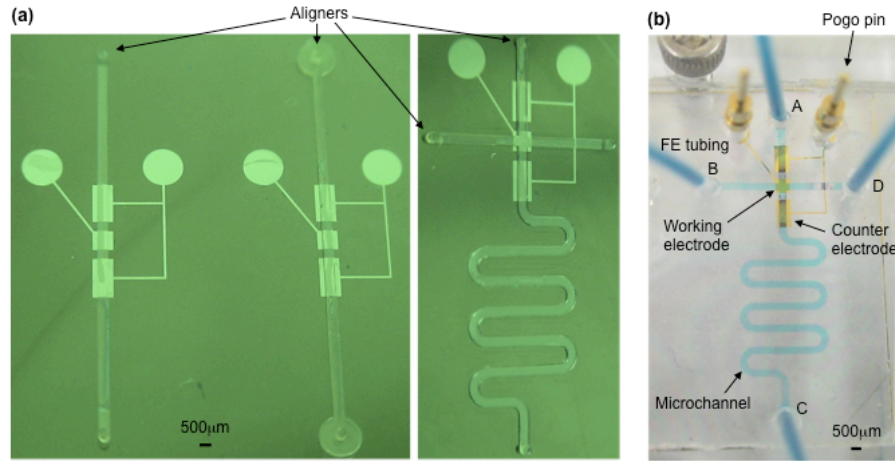


Figure 15: Device and packaging. (a) Fabricated aligners on prototype mold. (b) Blue dye solution occupying a leak-tight cross-channel device. PE tubing was inserted. In experiment, enzyme solution for post-fabricated assembly flowed A→C, and substrate solution (SAH) subsequently flowed B→D.

Section 3 Experimental methods

This section describes the methods employed to functionalize the microfluidic device with active *pfs* enzyme.

Sub-section 1 Enzyme assembly and enzymatic reactions

After leak testing of the assembled microfluidic chip, the microchannel and all the connecting tubing were rinsed with DI water at 50 μL/min flow rate for 30 minutes. Then, Bovine Serum Albumin (BSA) solution (1 % (w/v) in PBS buffer) was pumped into the microchannel at 3 μL/min flow rate for 2 hours to block non-specific binding. After PBS buffer rinsing for 15 min at 5 μL/min flow rate, *pfs*-chitosan conjugate solution was pumped at the same flow rate until the microchannel was completely filled before the pump was stopped. For all the control experiments to test the background signals, no electrical signal was applied to the working electrode during incubation of 240 seconds, as shown in Figure 17. The *pfs*-chitosan conjugate solution was then drained from the system, and the electrodeposited *pfs*-chitosan conjugate was washed with PBS buffer at 5 μL/min flow rate for 30 min. Next, enzymatic reactions were performed by

continuously pumping the SAH substrate solution (1mM SAH in 50mM sodium phosphate buffer, pH 7.2) for 2hr at 0.4, 1 and 4 μ L/min flow rates by a Genie Plus syringe pump. During the second hour at each flow rate, samples were collected every 20 min. They were then extracted with chloroform and stored at -20°C before analyzing via HPLC.

For the experiments to test the overall conversion by site-specifically assembled enzyme and non-specifically assembled enzyme, an electrical signal of constant current density 3 A/m² was applied to maintain negative bias voltage on the working electrode for 240 seconds, while a second electrode served as the counter electrode. All other steps followed the same aforementioned procedure.

Section 4 Results

Sub-section 1 Quantification and simulation of interconnect dead volume

To better understand the degree to which interconnect dead volume affects the system response at a specific reaction site, the changes in fluorescent dye intensity in the microchannel under flow were measured and quantified, at a point 8.75 mm downstream of the interconnect point over the active electrode (Figure 16(a)). The interconnect reservoir is 2 mm in diameter and 0.15 mm high, and the microchannel is 0.5 mm wide. The upstream external tubing was first filled with dye solution (Cy5) before inserting into the PDMS chip. A syringe pump pumped the dye solution into the microchannel at 1 μ L/min flow rate, and a fluorescent microscope simultaneously recorded the dye intensity over the electrode. The microscope images were converted into grayscale images and processed by ImageJ software (National Institutes of Health). As a

comparison, quantification was also performed for a microchannel of the same dimension without the interconnect reservoir (Figure 16 (b)).

Figure 16 (c) shows the changes in relative intensity over the electrode for a microchannel with interconnect reservoirs (pink solid line), and for a microchannel without interconnect reservoirs (blue dashed line). The left portion of the curves shows that it takes about 50 sec for the dye solution to reach the electrode. The right portion of the curves shows that in the microchannel with the interconnect reservoir, the dye intensity increases from 10% to 90% in 61 sec, while in the microchannel without interconnect reservoir it only takes 32 sec. The intensity difference over time in the microchannels with and without reservoir (Figure 16 (e), blue line) differs for more than 100 sec before it plateaus at the maximum value of 0.32.

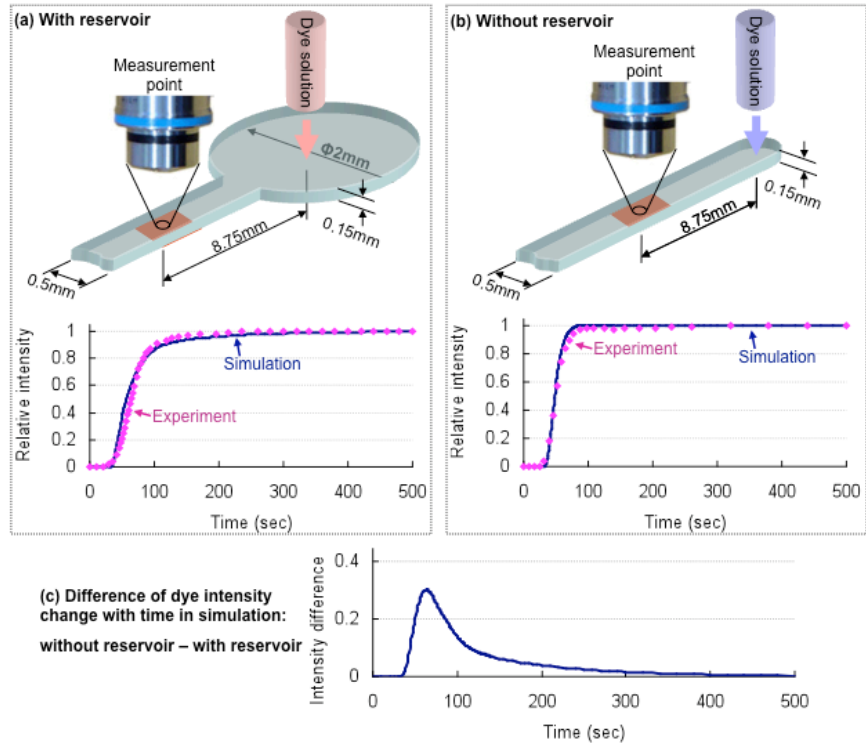


Figure 16: The residence time distribution for channels with, and without, reservoirs. Dye solution was monitored over electrode patches 12mm downstream the microchannels. (a) With reservoir. Dye intensity increasing from 10% to 90% takes 61 sec in experiment and 75 sec in simulation. (b) Without reservoir. Dye intensity increasing from 10% to 90% takes 32 sec in experiment and 25 sec in simulation. (c) The simulated difference of intensity change from the interconnect configuration with, and without, reservoir.

Finite element simulation was also performed to investigate the effects of the interconnect reservoir on the system response at the same location as in the experimental quantification. This simulation was performed using COMSOL Multi-Physics by modeling the switching of the incoming flow to dye solution at the interconnection point, and by integrating the dye intensity over the electrode. The left portion of the simulation curves (Figure 16 (d)) shows that it also takes about 35 sec for the dye solution to reach the electrode. The longer response time in this portion of the experiments is probably due the lag associated with pump startup and the extra tubing connecting the syringe pump. The right portion of the simulation curves shows that for a microchannel with an interconnect reservoir, it takes 75 sec for the dye intensity to increase from 10% to 90%

(Figure 16 (d), solid pink line), while for a microchannel without an interconnect reservoir it only takes 25 sec (Figure 16 (d), dashed blue line). The pink open line in Figure 16 (e) is the intensity difference in the microchannels with and without reservoir over time, which shows that the intensity over this specific electrode site differs for more than 100 sec before it reaches plateau with the maximum value 0.30. The shorter time to reach plateau for the microchannel with reservoir in the experiments is probably because of the pump. The flow driven by our syringe pump is not strictly continuous, but advances in a step-wise manner that is disadvantageous in applications where smooth continuous flow is desired.

Together, both the experimental quantification and the finite element simulation confirm that the system response (as measured downstream at the reaction site) has improved 2-3X by eliminating the dead volume in interconnect reservoirs, therefore avoiding the homogenous parasitic reactions in the dead volume.

Sub-section 2 Quantification of parasitic reactions and overall analysis

Part 1 Enzyme reaction and controls

To determine the benefit of the design changes detailed above which focus on microfluidics, enzymatic conversions in these various designs were compared to test the effects of parasitic reactions. This is schematically indicated in Figure 17 for the cases of (1) single channel with interconnect reservoirs, (2) single channel without interconnect reservoirs and (3) cross channel without reservoirs. The microchannels were first filled with *pfs* enzyme solution, and then incubated in the enzyme solution in a static state for 4min without applying an electrical signal to the assembly site (no electrodeposition). Next, enzyme solution was drained from the microchannel, and buffer solution was

introduced to rinse the channel. Finally, enzymatic substrate SAH was introduced, and the downstream solution was collected for analysis by HPLC.

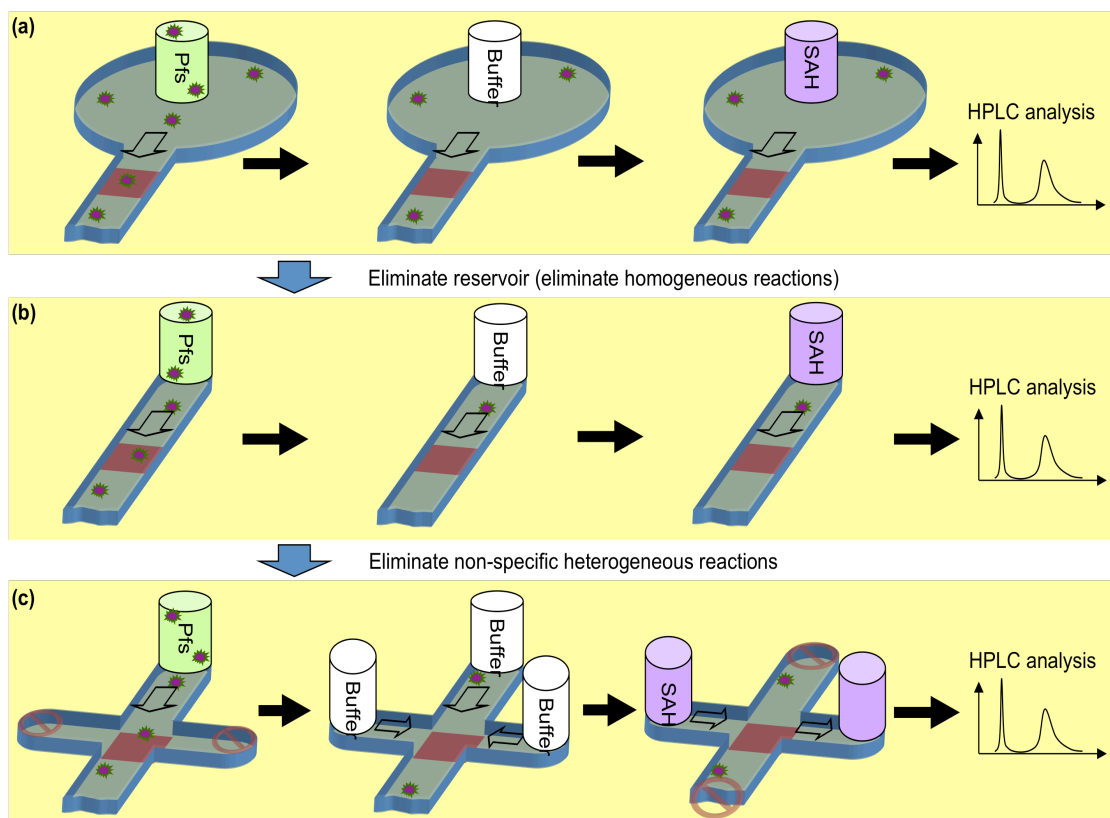


Figure 17: Minimization of parasitic reactions. To test the background signal by non-specifically bound enzyme, *pfs* enzyme solution was introduced without electro-assembly followed by buffer rinsing, then enzymatic substrate SAH was introduced and collected downstream to be analyzed by HPLC. (a) → (b) Eliminating dead volume in interconnect reservoir and thereby eliminating homogeneous reactions). (b) → (c) Eliminating non-specific binding of enzyme to channel walls and thereby minimizing heterogeneous reactions.

The experimental results in Figure 18 show that in the case of the single channel with reservoirs, the conversion of SAH into SRH and adenine was $44.5 \pm 2.9\%$, $19.3 \pm 0.4\%$ and $5.0 \pm 0.3\%$ at $0.4\mu\text{L}/\text{min}$, $1\mu\text{L}/\text{min}$ and $4\mu\text{L}/\text{min}$ flow rates, respectively. In the case of single channel without reservoirs, the conversion was $29.7 \pm 1.8\%$, $13.4 \pm 0.7\%$ and $4.1 \pm 0.3\%$ at $0.4\mu\text{L}/\text{min}$, $1\mu\text{L}/\text{min}$ and $4\mu\text{L}/\text{min}$ flow rates, respectively. In the case of

cross channel without reservoirs, the conversion was $13.3 \pm 0.2\%$, $6.8 \pm 0.3\%$ and $1.5 \pm 0.2\%$ at $0.4\mu\text{L}/\text{min}$, $1\mu\text{L}/\text{min}$ and $4\mu\text{L}/\text{min}$ flow rates, respectively.

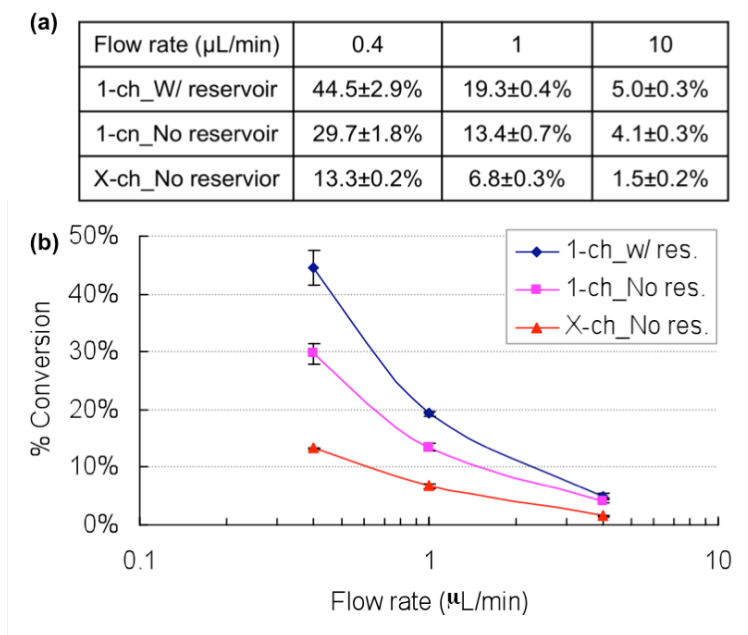


Figure 18: Background signals (parasitic enzymatic conversion) at different flow rates. *pfs* enzyme solution was introduced without electro-assembly followed by buffer rinsing, then enzymatic substrate SAH was introduced and collected downstream to be analyzed by HPLC. Legend: 1-ch_w/ res.: single channel with interconnect reservoirs (blue); 1-ch_No res.: single channel without interconnect reservoirs (purple); X-ch_No res: cross-channel without interconnect reservoirs (red).

Combined, these results demonstrate that by eliminating the reservoirs, the background signal from homogeneous parasitic reactions in the dead volume of interconnects decreases by 33%. By separating the flow directions with the cross channel configuration, the background signals from heterogeneous parasitic reactions on the microchannel walls further decreases by 63%. The total decrease of background signal from the configuration of Figure 17 (a) to that of Figure 17 (c) is 65~70% for the three flow rates tested.

Part 2 Enzyme conversion signal/background

To better understand the improvements realized by eliminating interconnect dead volume and separating the flow directions for sequential enzymatic reactions, site-specific heterogeneous enzymatic reactions on the assembly electrode were also performed side by side to compare with the control experiments. The experiments differ from the control experiments only in that an electrical signal of 3A/m^2 current density was applied to electrodeposit *pfs*-chitosan conjugate onto the assembly electrodes during the 4-min incubation of enzyme solution in the channels. The experiments were performed at $0.4\mu\text{L/min}$ flow rate for all the three configurations shown in Figure 17. The enzyme solution for all the experiments and controls was from the same batch, while the conjugate solution was made right before experiments. The background signal was taken from Figure 18 at the flow rate of $0.4\mu\text{L/min}$.

The experiment results in Figure 19 show that in the case of the single channel with reservoirs, the site-specific conversion is $32.0 \pm 1.6\%$ and the background signal is as high as $44.5 \pm 2.9\%$ yielding a signal/background (S/B) ratio of 0.72. In the case of the single channel without reservoirs design, the site-specific conversion is $38.1 \pm 0.6\%$ while the background signal is $29.7 \pm 1.8\%$ with the S/B ratio of 1.28. In the case of the cross channel without reservoirs design, the site-specific conversion is $32.3 \pm 3.5\%$ while the background signal is as low as $13.4 \pm 0.7\%$ with the S/B ratio of 2.43. The crosshatched area in Figure 19 (X-ch_No res) represents calculated missing reaction correction due to a slight reduction in electrode area upon alignment of intersection channels onto electrode. Note, however, the electrode with only 0.75mm^2 area represents only 1% of the total microchannel surface (77.15mm^2), and the volume above the electrode site ($0.11\mu\text{L}$) represents only 2.5% of the total microenvironment volume

(4.45 μ L). Therefore, the conversion on the enzyme-activated electrode is more than two orders of magnitude faster per unit area than the background signal resulting from either parasitic mechanism.

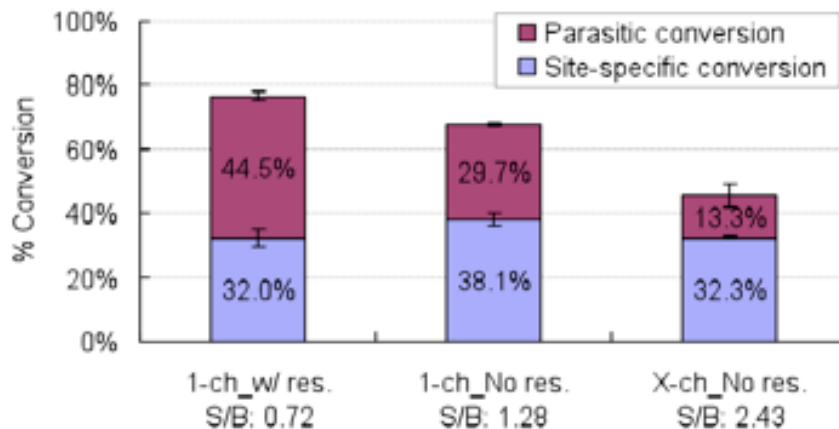


Figure 19: Total conversions in devices with electrodeposited *pfs*. Conversion by non-specifically bound enzymes is in blue, and conversion by site-specifically assembled enzymes is in red. For the non-specific conversion, no electrical signal was applied (no *pfs*-chitosan conjugate deposited). For the total conversion, an electrical signal of 3A/m² current density was applied for 4min (*pfs*-chitosan conjugate assembled onto 0.75 mm² sites). Enzymatic reaction was performed at 0.4 μ L/min flow rate.

In summary, these results demonstrate that by utilizing our packaging and experimental strategies to minimize the parasitic reactions in interconnect dead volume and by non-specific binding on microchannel walls, the signal-to-background ratio of sequential enzymatic reactions was improved from 0.72 to 2.43.

Section 5 Discussion

Estimation of enzyme specific activity was reported previously [16]. The enzyme specific activity for the *pfs*-chitosan conjugate assembled on the electrode in this paper (0.35 μ mol SAH/ min/ mg *pfs*) is lower than what was estimated in the previous publication (3.7 μ mol SAH/ min/ mg *pfs*). The difference might be due to several

reasons. First, the enzyme solution used here was from a different batch prepared at different time that might have different specific activity. Second, the EF-BioMEMs chip used here has a different configuration that might result in different activity after enzyme assembly. The chip design in Figure 15 consists of two counter electrodes besides the working electrode for enzyme assembly. During electrodeposition, this configuration might generate higher pH gradient at the working electrode surface, thereby deactivating the enzyme activity. Nonetheless, the estimated specific activity is within the range of reported *pf*s specific activities in the literature that vary over three orders of magnitude [4][6][20]. Importantly, given the enzyme specific activity and flow rate conditions, the purpose of suppressing parasitic reactions has been demonstrated by the decreasing background signal and increasing S/B ratio, as shown in Figure 18 and Figure 19, while the site-specific conversions remained at the same level.

The use of chitosan as an intermediary interface allows for the programmable assembly of enzymes in a microfluidic network, making this EF-BioMEMs platform both versatile and functional [5][24]. By improving the ability to specify the site of the individual enzymatic reactions, these modifications allow for the construction of the complex networks needed to simulate biologically relevant pathways. In these networks, each enzymatic step would be catalyzing a specific reaction with known conversion efficiency. The conversation rate of each step could be measured independently, and the conversion action would be attributable only the specifically bound enzyme, with minimal side-reactions.

Advanced methods for reducing parasitic reactions can be further developed. Homogenous parasitic reactions could be addressed by the use of low dead-volume

interconnect designs to interface the microfluidic channel with the external pumping and fluid delivery. By incorporating in-line valves for flow control, it is possible to envision purging flows which would flush the channel areas of any non-specifically bound enzyme. Additionally, through stronger and longer chemical pretreatment of the microchannel walls than the BSA solution used here, it might be possible to further repel enzyme bounding and thereby eliminate heterogeneous parasitic reactions.

Section 6 Conclusion

In summary, this work demonstrates a novel packaging technique to minimize the homogeneous parasitic reactions in the dead volume of packaging interconnects and an experimental strategy to minimize heterogeneous parasitic reactions due to non-specific binding on microchannel walls. Our experiment and simulation results prove that the combined strategies of fabricating packaging aligners to avoid the interconnect reservoirs and separating flow directions for enzyme immobilization and the subsequent enzymatic reactions are efficient in minimizing the background noise up to 70%. These strategies increase the signal-to-background ratio from 0.72 to 2.43 for the given chip design and enzyme activity. These techniques can be easily applied to versatile microfluidic chips to minimize cross-contamination in sequential biochemical reactions.

Chapter 4: Materials & Methods

Section 1 Chemicals and Materials

The materials used were similar to those used in previous works ^{[38][39][40]}. These materials were stored in the Payne, Bentley, and Rubloff laboratories at University of

Maryland, College Park, and the FabLab facilities in the Maryland Nanocenter. These materials are listed in Table 4 below:

Table 4: Chemicals and Materials List

Material	Application	Source
Silicon wafers	Substrates for SU8 processing	University Wafer
Gold	Microchannel electrode material	Kurt Lesker
Chromium	Adhesion layer to allow for gold electrode application to glass substrate	Kurt Lesker
Polydimethylsiloxane (PDMS), aka Sylgard 184	Construction material for microchannel	Robert McKweon
Microbore PTFE tubing, 0.022" (0.56mm) ID	Compatible tubing to connect microchannels to pumps and pressure supply	Cole Parmer, P/N HW-06417-21
PE tubing	Biochemical liquid handling	Instech Laboratories
Steel couplers (25ga, 20ga)	Novel interconnect fabrication	Instech Laboratories
Single-Use syringes/BD Needle Combinations	Biochemical liquid handling	VWR
Microcentrifuge tubes	Biochemical liquid storage	VWR
Plain glass microslides	Substrate for the microchannel	VWR
Syringe Pump	Controlled delivery of fluid to microfluidic chip	Kent Scientific, Genie Plus Infusion/Withdrawal Pump
Acetone/Methanol/IPA	Wafer cleaning solvents	Fisher Chemical
SU8-50 photoresist	Construction material for valve mold	MicroChem
SU8 Developer	Developer for SU8-50 photoresist	MicroChem
Shipley 1813 Photoresist	Gold & Chromium Photoresist	MicroChem
Shipley 352 Developer	Developing agent for Shipley 1813 Photoresist	MicroChem
Transene TFA etchant	Gold etchant solution	MicroChem
Transene 1020	Chromium etchant solution	MicroChem
Luria Broth	E. coli culture medium	Becton Dickinson
Ampicillin	E. coli culture medium	Fisher Chemical
Sodium Chloride	E. coli culture medium	Fisher Chemical
isopropyl b-D-thiogalactopyranoside (IPTG)	Enzyme purification	Sigma Aldrich
Imidazole	Enzyme purification	Sigma Aldrich
Bleach	Disinfectant	James Austin Co.
Sodium cyanoborohydride	Stabilize <i>pfs</i> -chitosan binding	Sigma Aldrich
Tyrosinase (from mushroom)	Manufacturer reported activity: 1,530 units/mg solid; formation of tyrosine tag for enzyme conjugation to chitosan	Sigma Aldrich
BSA	Bovine Serum Albumin, to block non-specific chitosan binding to microchannel	Sigma Aldrich
Chitosan	Minimum 85 % deacetylated chitin; molecular weight 200,000 g/mol, from crab shells	Sigma Aldrich
SAH	S-adenosylhomocysteine, <i>pfs</i> substrate	Sigma Aldrich
Non-fat dry milk	To discourage non-specific chitosan bonding, and stabilize pH near optimum value.	BioRad
Hydrochloric Acid	Hydrochloric Acid, for channel cleaning	J.T. Baker
Phosphate Buffered Saline (PBS) (2.7mM KCl, 137mM NaCl, 1.5mM KH ₂ PO ₄ , 8.1mM Na ₂ HPO ₄ , pH 7.5)	Buffer solution to flush out chitosan conjugate without causing premature precipitation, and stabilize the electrodeposited chitosan. Autoclaved before use.	Sigma Aldrich

ddH ₂ O	Doubly deionized water, for channel rinsing Autoclaved before use	Made in-house
Chloroform	Sample stabilization	Fisher Chemical
DI Water (HPLC grade)	HPLC solvent component	Fisher Chemical
Acetonitrile (HPLC grade)	HPLC solvent component	Fisher Chemical

Section 2 Methods of Preparation

Sub-section 1 Plasmid construction

pTrcHis-*pfs*-Tyr plasmid construction has been reported elsewhere ^[5]. Briefly, the plasmid was constructed by PCR amplification of *pfs* from *E. coli* wild type strain W3110. Following digestion, the PCR products were extracted by gel purification and inserted into pTrcHisC (Invitrogen). DNA sequencing was performed to verify construct integrity. The plasmid was transformed into *E. coli* DH5 α (defective *LuxS* strain).

Sub-section 2 Purification of (His)₆-*pfs*-(Tyr)₅

The procedure for preparation of purified (His)₆-*pfs*-(Tyr)₅ has been covered elsewhere ^[5], but is included here for completeness. *E. coli* DH5 α containing pTrcHis-*pfs*-Tyr was cultured at 37°C and 250 rpm in LB medium supplemented with ampicillin at 50 μ g/mL concentration. When the OD_{600nm} reached 0.5-0.6, IPTG was added to induce enzyme production at a final concentration of 1mM IPTG. After an additional 5 hr, the culture was centrifuged for 10min at 10,000g's, and the cell pellet stored at -20°C. The thawed pellet was re-suspended in PBS + 10mM imidazole, pH 7.5, placed in an ice-water bath, and the cells lysed by sonication (Fisher Scientific Sonic Dismembrator 550). The lysed cells were centrifuged for 10min at 16,000g to remove insoluble cell debris, and the supernatant filtered through 0.22 μ m PES filter. The enzyme was purified from the filtered soluble cell extract by immobilized metal-ion affinity chromatography (IMAC) using a 5mL HisTrap chelating column (Amersham Biosciences). Prior to loading the filtered extract, the column was charged with Ni²⁺ ions using 0.1M NiSO₄, washed with

deionized water, and equilibrated with 3 column volumes (CVs) of 20mM sodium phosphate, 250mM NaCl, 10mM imidazole, pH 7.4. After loading the filtered extract, the column was washed with 3 CVs of the previous buffer, washed again with 3 CVs of 20mM sodium phosphate, 250mM NaCl, 50mM imidazole, pH 7.4, and the protein was eluted using 1.5 CVs of 20mM sodium phosphate, 250mM NaCl, 350mM imidazole, pH 7.4. All steps were performed at 2mL/min (1cm/min linear velocity). The eluted sample was dialyzed overnight (16hr) at 4°C into PBS. Purified protein concentration was determined by UV/vis spectrophotometry (DU 640, Beckman, Fullerton, CA) using UV light at 280nm wavelength. The protein solution was mixed 2:1 with glycerol, aliquoted and stored at -80°C.

Sub-section 3 *pfs*-chitosan conjugate preparation

Chitosan, enzyme *pfs*, and *pfs*-chitosan conjugate preparation procedures were reported elsewhere^{[14][16]}. Briefly, Chitosan solution was prepared by dissolving chitosan flakes in HCl solution at pH ~ 2 overnight, then the pH was adjusted to pH 4.8 by adding 1 M NaOH dropwise before being filtered and stored at 4°C. Plasmid pTrcHis-*pfs*-Tyr was first constructed by PCR amplification of *pfs* from *E. coli* wild type strain W3110. Following digestion, the PCR products were extracted by gel purification and inserted into pTrcHisC (Invitrogen). DNA sequencing was performed to verify construct integrity. The plasmid was transformed into *E. coli* DH5 α (defective *luxS* strain). *E. coli* DH5 α containing pTrcHis-*pfs*-Tyr was cultured and enzyme production was induced before the cells were lysed by sonication. Next, the enzyme was purified by ion-metal affinity chromatography (IMAC) before being mixed 2:1 with glycerol, divided into aliquots, and stored at -80°C. The conjugate was prepared by incubating enzyme *pfs*,

tyrosinase, and chitosan in sodium phosphate buffer for 2hr at room temperature followed by incubation in sodium cyanoborohydride for 30min to stabilize *pfs*-chitosan binding.

Section 3 Analysis of enzymatic reaction products

A Waters Spherisorb Silica column (250 × 4.6mm) with 5mm beads (80 Å pore) was used in reversed-phase mode with 5mL sample injection size and a mobile phase of 70:30 acetonitrile: water at 0.5mL/min. Only HPLC-grade chemicals were used for the mobile phase. The HPLC system consisted of two Dynamax model SD-200 pumps (with 10mL pump heads and mixing valve) and a Dynamax Absorbance Detector model UV-D II, and data was analyzed using Star 5.5 Chromatography Software (Rainin). Conversion was calculated from elution data at 210nm absorbance.

Chapter 5: Discussion

Section 1 Summary of Key Findings

This thesis work demonstrates the biochemical inhibition of the *pfs* enzyme in a microfluidic device. *Pfs* is the first enzyme conversion step in the metabolic pathway used by bacteria during quorum sensing, so this achievement demonstrates a method to disrupt bacterial communication. The *pfs* enzyme was spatially assembled at a defined site within an enzyme-functionalized microfluidic system and controllably exposed to varying concentrations of a substrate analog inhibitor, MT-DadMe-Immucillin-A. The result was a decrease in enzyme conversion activity in a manner comparable to that observed in larger-scale well-mixed experimental configurations. This demonstrates that

the EF-BioMEM system can be used to screen other compounds for the potential as enzyme inhibitors of the quorum-sensing pathway.

This thesis work also describes design improvements that were implemented to reduce unintended enzyme reactions within the microfluidic device, and thus improves the overall system performance by increasing the signal-to-background ratio. Unintended reactions were found to occur because of conversion activity from enzyme trapped within the dead volume of the device, and enzyme non-specifically bound to the sidewalls of the microchannel. By implementing a novel packaging scheme, it was possible to eliminate the interconnect reservoir and reduce the background signal from homogenous reactions in the dead volume by 33%. A cross-channel geometry was designed which separated the flow paths of the enzyme during functionalized, from the substrate during conversion. This change in geometry reduced the background signals from unintended heterogeneous reactions on the microchannel walls by an additional 63%. Together, these strategies increased the signal-to-background ratio from 0.72 to 2.43 for the chip design presented.

Section 2 Future Work

Now that it has been demonstrated that enzyme inhibition can be observed in this design of microfluidic device, it would be desirable to use it to screen other compounds for their efficacy as *pfs* inhibitors. Schramm's research has identified listed several other picomolar and femtomolar *pfs* inhibitors ^{[34][45][46][47][48]} which could be candidates for future study.

The Rubloff group at University of Maryland has done work to integrate on-chip pressure valves into the microfluidic network. These valves are modeled after those

described by Quake and Melin ^[49]. By employing these valves and the cross-channel geometry described in Section Chapter 3:Section 2Sub-section 2, it is possible to design a microfluidic network that separates the flow directions of the enzyme, the substrate, and the substrate/inhibitor mixture so that higher throughput screening operations are possible.

The issue of limited interaction between the flow stream and the assembled enzyme is addressed in Figure 12. It would be desirable to position the enzyme in a way that would maximize its interaction with the substrate to increase the amount of conversion. The Rubloff group has done work that involves fabricating a vertical chitosan membrane inside the microfluidic channel so that it is perpendicular to fluid flow. This membrane can be further functionalized with active enzyme. This geometrical rearrangement has been shown (unpublished work) to increase enzyme conversion, and would improve the signal response in subsequent inhibitor screening studies.

Chapter 6: Appendix

Section 1 Cost Analysis

One intended application of a biofunctionalized microfluidic chip would be as a cartridge in applications unit for biochemical analysis. To evaluate the feasibility of mass production of these microfluidic chips, a basic manufacturing cost analysis is presented in Table 5. Each microchip costs \$7.74/chip, and would require \$3.71 worth of chemicals (not including enzyme) to biofunctionalized. The typical processing time took 2 days, was done in the FabLab facility at the Maryland NanoCenter by a single worker.

Table 5: Manufacturing Cost Analysis

		Batch Cost	Cost per unit	Information Source
Microfluidics	Glass slides	\$34.75/pack	\$ 0.48	VWR
	Gold	\$950/oz	\$ 6.50	Kurt Lesker & Gold Price sheet
	Chromium	\$2075/kg	\$ 0.02	Kurt Lesker & Cr Price sheet
	PDMS	\$305.47/kit	\$ 0.67	Robert McKweon Company
	Mask	\$34/mask	\$ 0.07	CAD/Art Services
			\$ 7.74	
Immobilization	Chitosan	\$542/kg	\$ 2.71	Sigma Aldrich
	PBS	\$150.50/kit	\$ 0.30	Sigma Aldrich
	HCl Acid	\$72.90/2.5L	\$ 0.58	Fisher
	NaOH	\$22.90/L	\$ 0.11	Fisher
			\$ 3.71	
Equipment	Microscope	\$300	\$ 0.02	est. from Ebay resale cost
	Vacuum chamber	\$120	\$ 0.12	from Aquatic EcoSystems
	Vacuum pump	\$500	\$ 0.50	from Aquatic EcoSystems
	Evaporator	\$40,000	\$ 44.44	from FabLab staff
	UV Exposure	\$15,000	\$ 2.50	from FabLab staff
	Voltmeter	\$1,000	\$ 0.06	Keithley
	Oven	\$300	\$ 0.30	est. from Ebay resale cost
			\$ 47.94	
	Material Costs		\$ 59.39	

Chapter 7: References

1. A.A.S. Bhagat, P. Jothimuthu, A. Pais, I. Papautsky, *Journal of Micromechanics and Microengineering* 17:42-49 (2007).
2. U. Bilitewski, M. Genrich, S. Kadow, G. Mersal, *Analytical and Bioanalytical Chemistry* 377:556-569 (2003).
3. A.M. Christensen, D.A. Chang-Yen, B.K. Gale, *Journal of Micromechanics and Microengineering* 15:928-934 (2005).
4. J.A. Duerre, *Journal of Biological Chemistry* 237:3737-& (1962).
5. R. Fernandes, H.M. Yi, L.Q. Wu, G.W. Rubloff, R. Ghodssi, W.E. Bentley, G.F. Payne, *Langmuir* 20:906-913 (2004).
6. A.J. Ferro, A. Barrett, S.K. Shapiro, *Biochimica Et Biophysica Acta* 438:487-494 (1976).
7. C.K. Fredrickson, Z.H. Fan, *Lab on a Chip* 4:526-533 (2004).
8. B.L. Gray, S.D. Collins, R.L. Smith, *Sensors and Actuators a-Physical* 112:18-24 (2004).
9. A. Han, M. Graff, O. Wang, A.B. Frazier, *Ieee Sensors Journal* 5:82-89 (2005).
10. D. Janasek, J. Franzke, A. Manz, *Nature* 442:374-380 (2006).
11. S. Kim, B. Huang, R.N. Zare, *Lab on a Chip* 7:1663-1665 (2007).
12. B.S. Ku, J.H. Cha, A. Srinivasan, S.J. Kwon, J.C. Jeong, D.H. Sherman, J.S. Dordick, *Biotechnology Progress* 22:1102-1107 (2006).
13. S.W. Lee, S.S. Lee, *Microsystem Technologies-Micro-and Nanosystems-Information Storage and Processing Systems* 14:205-208 (2008).
14. A.T. Lewandowski, D.A. Small, T.H. Chen, G.F. Payne, W.E. Bentley, *Biotechnology and Bioengineering* 93:1207-1215 (2006).
15. Z. Long, Z. Shen, D. Wu, J. Qin, B. Lin, *Lab on a Chip* 7:1819-1824 (2007).
16. X. Luo, A.T. Lewandowski, H. Yi, G.F. Payne, R. Ghodssi, W.E. Bentley, G.W. Rubloff, *Lab on a Chip* 8:420-430 (2008).
17. J.C. McDonald, G.M. Whitesides, *Acc Chem Res* 35:491-499 (2002).
18. J.J. Park, X.L. Luo, H.M. Yi, T.M. Valentine, G.F. Payne, W.E. Bentley, R. Ghodssi, G.W. Rubloff, *Lab on a Chip* 6:1315-1321 (2006).
19. S.R. Quake, A. Scherer, *Science* 290:1536-1540 (2000).
20. E.D. Ragione, M. Porcelli, M. Cartenifarina, V. Zappia, *Biochemical Journal* 232:335-341 (1985).
21. Y.C. Tan, V. Cristini, A.P. Lee, *Sensors and Actuators B-Chemical* 114:350-356 (2006).
22. T. Thorsen, S.J. Maerkl, S.R. Quake, *Science* 298:580-584 (2002).
23. P.L. Urban, D.M. Goodall, N.C. Bruce, *Biotechnology Advances* 24:42-57 (2006).
24. L.Q. Wu, H.M. Yi, S. Li, G.W. Rubloff, W.E. Bentley, R. Ghodssi, G.F. Payne, *Langmuir* 19:519-524 (2003).
25. H.M. Yi, L.Q. Wu, W.E. Bentley, R. Ghodssi, G.W. Rubloff, J.N. Culver, G.F. Payne, *Biomacromolecules* 6:2881-2894 (2005).
26. V. Sperandio, A. G. Torres and J. B. Kaper, *Mol. Microbiol.*, 2002, 43, 809–821.
27. V. Sperandio, A. G. Torres, J. A. Giron and J. B. Kaper, *J. Bacteriol.*, 2001, 183, 5187–5197.

28. Hooshangi and Bentley. From unicellular properties to multicellular behavior: bacteria quorum sensing circuitry and applications. *Current Opinion in Biotechnology* (2008) vol. 19 (6) pp. 550-555.
29. Zhu et al. Quorum-sensing regulators control virulence gene expression in *Vibrio cholerae*. *Proceedings of the National Academy of Sciences* (2002) vol. 99 (5) pp. 3129.
30. Balestrino et al. Characterization of type 2 quorum sensing in *Klebsiella pneumoniae* and relationship with biofilm formation. *J Bacteriol* (2005) vol. 187 (8) pp. 2870-2880.
31. Ren et al. Inhibition of biofilm formation and swarming of *Escherichia coli* by (5Z)-4-bromo-5-(bromomethylene)-3-butyl-2 (5H)-furanone. *Environmental Microbiology* (2001) vol. 3 (11) pp. 731-736.
32. Lennen. Inhibitors of Autoinducer-2 Quorum Sensing and Their Effect on Bacterial Biofilm Formation. drum.umd.edu (2007).
33. Lewandowski. Assembly of Quorum Sensing Pathway Enzymes onto Patterned Microfabricated Devices. (2007).
34. Singh et al. Femtomolar transition state analogue inhibitors of 5'-methylthioadenosine/S-adenosylhomocysteine nucleosidase from *Escherichia coli*. *Journal of Biological Chemistry* (2005) vol. 280 (18) pp. 18265-18273.
35. W. Blanch and S. Clark. *Biochemical engineering*. (1997) pp. 702.
36. Thorsen et al. Microfluidic large-scale integration. *Science* (2002) vol. 298 (5593) pp. 580-4.
37. Maryland Nanocenter, Kim Engineering Bldg., University of Maryland, College Park, MD 20742.
38. Lewandowski et al. Tyrosine-based "Activatable Pro-Tag": Enzyme-catalyzed protein capture and release. *Biotechnology and Bioengineering* (2006) vol. 93 (6) pp. 1207-1215.
39. Luo et al. Programmable assembly of a metabolic pathway enzyme in a pre-packaged reusable bioMEMS device. *Lab on a Chip* (2008).
40. Luo et al. Design optimization for bioMEMS studies of enzyme-controlled metabolic pathways. *Biomed Microdevices* (2008) vol. 10 (6) pp. 899-908.
41. Holden et al. Patterning enzymes inside microfluidic channels via photoattachment chemistry. *ANALYTICAL CHEMISTRY-WASHINGTON DC-* (2004) vol. 76 (7) pp. 1838-1843.
42. Ismagilov et al. Microfluidic arrays of fluid-fluid diffusional contacts as detection elements and combinatorial tools. *ANALYTICAL CHEMISTRY-WASHINGTON DC-* (2001) vol. 73 (21) pp. 5207-5213.
43. Mao et al. Design and characterization of immobilized enzymes in microfluidic systems. *Anal. Chem* (2002) vol. 74 (2) pp. 379-385.
44. Eteshola and Leckband. Development and characterization of an ELISA assay in PDMS microfluidic channels. *Sensors & Actuators: B. Chemical* (2001).
45. Singh et al. Transition state structure of 5'-methylthioadenosine/S-adenosylhomocysteine nucleosidase from *Escherichia coli* and its similarity to transition state analogues. *Biochemistry-Columbus* (2005) vol. 44 (35) pp. 11647-11659.

46. Singh et al. Structure and Inhibition of Quorum Sensing Target from *Streptococcus pneumoniae*. *Biochemistry* (2006).
47. Singh and Schramm. Transition-State Analysis of *S. pneumoniae* 5'-Methylthioadenosine Nucleosidase. *J. Am. Chem. Soc* (2007).
48. Lee et al. Structural rationale for the affinity of PICO-and femtomolar transition state analogues of *E. coli* 5'-/s- nucleosidase. *Journal of Biological Chemistry* (2005).
49. Melin and Quake. Microfluidic large-scale integration: the evolution of design rules for biological automation. *Annual review of biophysics and biomolecular structure* (2007) vol. 36 pp. 213-31.
50. Alfaro et al. Synthesis of LuxS Inhibitors Targeting Bacterial Cell– Cell Communication. *Org. Lett* (2004) vol. 6 (18) pp. 3043-3046.
51. Shen et al. Design and synthesis of substrate and intermediate analogue inhibitors of S-ribosylhomocysteinase. *J Med Chem* (2006).
52. Cornell et al. Characterization of Recombinant *Escherichia coli* 5'-Methylthioadenosine/S-Adenosylhomocysteine Nucleosidase: Analysis of Enzymatic Activity and Substrate Specificity. *Biochemical and Biophysical Research Communications* (1996) vol. 228 (3) pp. 724-732.